bioRxiv preprint doi: https://doi.org/10.1101/2022.06.06.494981; this version posted June 7, 2022. The copyright holder for this preprint (which was not certified by peer review) is the author/funder, who has granted bioRxiv a license to display the preprint in perpetuity. It is made available under a CC-BY 4.0 International license.

PLK4 drives centriole amplification and apical surface area expansion in multiciliated cells

Gina M LoMastro[1], Chelsea G Drown[1], Aubrey L Maryniak[1], Cayla E Jewett[1], Margaret A Strong[1], Andrew J Holland[1]

[1]Department of Molecular Biology and Genetics, Johns Hopkins University School of Medicine, Baltimore, MD, USA

*Correspondence should be addressed to A.J.H: aholland@jhmi.edu

bioRxiv preprint doi: https://doi.org/10.1101/2022.06.06.494981; this version posted June 7, 2022. The copyright holder for this preprint (which was not certified by peer review) is the author/funder, who has granted bioRxiv a license to display the preprint in perpetuity. It is made available under a CC-BY 4.0 International license.

Abstract

Multiciliated cells (MCCs) are terminally differentiated epithelia that assemble multiple motile cilia used to promote fluid flow. To template these cilia, MCCs dramatically expand their centriole content during a process known as centriole amplification. In cycling cells, the master regulator of centriole assembly Polo-like kinase 4 (PLK4) is essential for centriole duplication; however recent work has questioned the role of PLK4 in centriole assembly in MCCs. To address this discrepancy, we created genetically engineered mouse models and demonstrated that both PLK4 protein and kinase activity are critical for centriole amplification in MCCs. Tracheal epithelial cells that fail centriole amplification accumulate large assemblies of centriole proteins and do not undergo apical surface area expansion. These results show that the initial stages of centriole assembly are conserved between cycling cells and MCCs and suggest that centriole amplification and surface area expansion are coordinated events.

bioRxiv preprint doi: https://doi.org/10.1101/2022.06.06.494981; this version posted June 7, 2022. The copyright holder for this preprint (which was not certified by peer review) is the author/funder, who has granted bioRxiv a license to display the preprint in perpetuity. It is made available under a CC-BY 4.0 International license.

Introduction

Multiciliated cells (MCCs) are specialized epithelial cells that line the surface of the respiratory tract, brain ventricles, and reproductive systems. MCCs contain tens to hundreds of motile cilia that collectively beat to drive fluid flow across epithelial surfaces. Each motile cilium is templated by a centriole or basal body that docks at the plasma membrane and extends a ciliary axoneme. Abnormalities in motile cilia assembly or function cause several pathologies, including chronic respiratory tract infections, hydrocephalus, and reduced fertility (Reiter and Leroux 2017; Spassky and Meunier 2017; Terre et al. 2019; Yuan et al. 2019).

In cycling cells, centriole duplication is tightly controlled so that a single new procentriole is created on the wall of each of the two parent centrioles during every cell cycle (Nigg and Holland 2018). By contrast, MCC progenitors with two parent centrioles produce tens to hundreds of new centrioles during their differentiation to generate the basal bodies required for multiciliogenesis. MCCs utilize two pathways to promote massive centriole amplification: a ‘centriole pathway’ where multiple procentrioles assemble on the wall of the two parent centrioles, and a ‘deuterosomal pathway’ where dozens of specialized structures called deuterosomes provide the nucleation sites for multiple procentrioles (Sorokin 1968; Steinman 1968; Brenner 1969; Kalnins and Porter 1969; Anderson and Brenner 1971; Klos Dehring et al. 2013; Al Jord et al. 2014; Revinski et al. 2018). MCC differentiation is defined by distinct stages (Al Jord et al. 2017). In mouse ependymal cells, procentrioles form around parent centrioles and deuterosomes during amplification (A) phase. Procentrioles elongate during growth (G) phase and detach from their growing platforms at disengagement (D) phase. Disengaged centrioles migrate and dock at the apical membrane to become basal bodies that form motile cilia during the multiple basal body (MBB) phase.

How MCCs control the final number of centrioles generated remains an open question. Centriole number scales with apical surface area in multiciliated mTECs and *Xenopus* embryonic epidermis (Nanjundappa et al. 2019; Kulkarni et al. 2021). In *Xenopus*, mechanical stretching forces help couple centriole number with MCC apical area

bioRxiv preprint doi: https://doi.org/10.1101/2022.06.06.494981; this version posted June 7, 2022. The copyright holder for this preprint (which was not certified by peer review) is the author/funder, who has granted bioRxiv a license to display the preprint in perpetuity. It is made available under a CC-BY 4.0 International license.

(Kulkarni et al. 2021). However, while mouse MCCs amplify centrioles in a single round of centriole biogenesis, *Xenopus* epidermal MCCs cells produce centrioles in two distinct waves (Al Jord et al. 2014; Kulkarni et al. 2021). Thus, it remains to be established whether similar or distinct mechanisms operate to set centriole numbers in mammalian MCCs.

Polo-like kinase 4 (PLK4) is the master regulator of centriole biogenesis and is required for centriole assembly in all cycling mammalian cell types studied (Bettencourt-Dias et al. 2005; Habedanck et al. 2005). During centriole duplication, CEP152 and CEP192 recruit PLK4 to the surface of the parent centrioles (Cizmecioglu et al. 2010; Hatch et al. 2010; Kim et al. 2013; Sonnen et al. 2013; Park et al. 2014). PLK4 kinase activity directs the assembly of STIL and SAS6 into a central cartwheel that provides the structural foundation for the new procentriole, and inhibition of PLK4 activity blocks centriole assembly (Dzhindzhev et al. 2014; Ohta et al. 2014; Kratz et al. 2015; Moyer et al. 2015). PLK4 is recruited to the surface of both parent centrioles and deuterostomes in MCCs (Nanjundappa et al. 2019). However, recent work has shown that inhibiting PLK4 kinase activity with the ATP-competitive small molecule centrinone has no impact on centriole amplification in mouse multiciliated ependymal cells or mTECs (Nanjundappa et al. 2019; Zhao et al. 2019). In addition, shRNA-mediated depletion of PLK4 modestly delays centriole assembly in mTECs but does not reduce the final number of centrioles produced or the fraction of cells forming motile cilia (Nanjundappa et al. 2019). These data suggest there are distinct requirements for PLK4 in promoting centriole assembly in cycling cells and differentiating mouse MCCs. However, PLK4 levels are upregulated ~20-fold in differentiating mTECs, and it remains plausible that partial inhibition or depletion of PLK4 is not sufficient to prevent centriole amplification in MCCs (Hoh et al. 2012).

In this study, we use genetic approaches to define the requirements of PLK4 protein and kinase activity for centriole amplification in MCCs. These genetic tools have the advantage of achieving highly specific and penetrant target engagement. In addition, we investigate the impact of blocking centriole amplification on the differentiation and

bioRxiv preprint doi: https://doi.org/10.1101/2022.06.06.494981; this version posted June 7, 2022. The copyright holder for this preprint (which was not certified by peer review) is the author/funder, who has granted bioRxiv a license to display the preprint in perpetuity. It is made available under a CC-BY 4.0 International license.

surface area scaling of MCCs. Our data show that PLK4 protein and kinase activity are required for centriole assembly in mouse MCCs, demonstrating that the early stages of centriole assembly are similar in cycling cells and MCCs. Moreover, we show that centriole amplification drives an increase in apical surface area in airway multiciliated cells, suggesting that increased centriole number is a central driver of surface area scaling in MCCs.

bioRxiv preprint doi: https://doi.org/10.1101/2022.06.06.494981; this version posted June 7, 2022. The copyright holder for this preprint (which was not certified by peer review) is the author/funder, who has granted bioRxiv a license to display the preprint in perpetuity. It is made available under a CC-BY 4.0 International license.

Results

Generation of a conditional loss-of-function allele of PLK4

To test the requirement of PLK4 for centriole amplification in multiciliated cells, we created mice with exon 5 of the *Plk4* gene flanked by *LoxP* recombination sites (hereafter $Plk4^{F}$ allele). Cre-mediated excision of exon 5 generates a *Plk4* allele (hereafter $Plk4^{\Delta}$ allele) lacking a large portion of the PLK4 kinase domain, including the DFG motif required for kinase activity. Splicing of *Plk4* exon 4 into exon 6 is predicted to generate a frame-shift that creates a premature termination codon at amino acid 119 **(Fig S1A)**.

Intercrosses of $Plk4^{F/\Delta}$ mice produced $Plk4^{F/F}$ and $Plk4^{F/\Delta}$ progeny but $Plk4^{\Delta/\Delta}$ animals were never observed **(Fig S1B)**. To validate the $Plk4^{F}$ allele, we inactivated PLK4 throughout the central and peripheral nervous system using Nestin-Cre. $Plk4^{F/F}$;Nestin-Cre animals developed severe microcephaly leading to a 35% reduction in telencephalic area at E14.5 **(Fig S1C,D)**. To examine how the loss of PLK4 disrupted centriole duplication *in vivo*, we analyzed dividing neural progenitor cells at the ventricular zone in E14.5 cortices. As expected, loss of PLK4 led to a dramatic decrease in centriole number **(Fig S1E)**. We conclude that $Plk4^{F}$ is a conditional loss-of-function allele of *Plk4*.

Ependymal cells lacking PLK4 fail to amplify centrioles

To test the impact of PLK4 loss in multiciliated cells, $Plk4^{F/F}$ and $Plk4^{F/+}$ ependymal cells were transduced with Adeno-associated-virus (AAV) expressing NLS-Cre-GFP (hereafter AAV-Cre). Ependymal cells were induced to differentiate and transduced cells expressing nuclear GFP were analyzed at various time points after infection **(Fig 1A, S1F)**. The frequency of FOXJ1+ ependymal cells at each time point was similar in $Plk4^{F/+}$ and $Plk4^{F/F}$ Cre+ cells **(Fig 1B)**. In addition, $Plk4^{F/F}$ and $Plk4^{F/+}$ cells formed deuterosomes at the same frequency **(Fig 1C)**, indicating that loss of PLK4 does not block the differentiation of multiciliated cells *in vitro*.

bioRxiv preprint doi: https://doi.org/10.1101/2022.06.06.494981; this version posted June 7, 2022. The copyright holder for this preprint (which was not certified by peer review) is the author/funder, who has granted bioRxiv a license to display the preprint in perpetuity. It is made available under a CC-BY 4.0 International license.

The PLK4 receptor CEP152 stained the surface of parent centrioles and deuterosomes in ependymal cells with or without PLK4 **(Fig S2A)**. To determine the extent of PLK4 depletion, we quantified the intensity of PLK4 on the deuterosomes of differentiating multiciliated cells. PLK4 abundance was reduced by 80% in Cre+ *Plk4*$^{F/F}$ ependymal cells compared to Cre+ *Plk4*$^{F/+}$ control cells **(Fig 1D,E)**. Consistent with PLK4 loss, deuterosomal recruitment of the PLK4 substrate and early centriole assembly factor STIL was abolished in Cre-expressing *Plk4*$^{F/F}$ ependymal cells **(Fig 1 F,G)**. These data show that similar to cycling cells, PLK4 is required to recruit STIL to the site of procentriole assembly in differentiating ependymal cells.

To evaluate the effect of PLK4 loss on centriole amplification in ependymal cells, we analyzed centriole number in disengagement phase (D phase) when individual centrioles can be resolved. Cre+ *Plk4*$^{F/+}$ ependymal cells amplified ~100 centrioles per cell, while most *Plk4*$^{F/F}$ ependymal cells failed to undergo centriole amplification and contained only the two parent centrioles that were present at the start of MCC differentiation **(Fig 2A,B)**. Consistently, Cre+ FOXJ1+ *Plk4*$^{F/F}$ ependymal cells rarely nucleated multicilia **(Fig 2C,D, Fig S2B,C)**.

To confirm that centriole assembly was blocked in ependymal cells lacking PLK4, we performed expansion microscopy on AAV-Cre transduced *Plk4*$^{F/+}$ and *Plk4*$^{F/F}$ ependymal cells. We observed procentrioles associated with both deuterosomes and parent centrioles in control cells but procentrioles were absent in ependymal cells lacking PLK4 **(Fig 2E,F)**. This confirms that PLK4 is required for the earliest stages of centriole assembly in ependymal MCCs.

Multiciliated ependymal cells are derived from a subset of neural progenitor cells (NPCs). Loss of centrioles in NPCs activates a USP28-53BP1-TP53 mitotic surveillance pathway that blocks NPC proliferation and indirectly depletes multiciliated cells (Lambrus et al. 2016; Phan et al. 2021). To enable the proliferation of NPCs lacking PLK4 and centrioles, we inactivated the mitotic surveillance pathway in *Plk4*$^{F/F}$;Nestin-Cre mice through knockout of USP28. While *Plk4*$^{F/F}$;Nestin-Cre mice died shortly after

bioRxiv preprint doi: https://doi.org/10.1101/2022.06.06.494981; this version posted June 7, 2022. The copyright holder for this preprint (which was not certified by peer review) is the author/funder, who has granted bioRxiv a license to display the preprint in perpetuity. It is made available under a CC-BY 4.0 International license.

birth, *Plk4*$^{F/F}$;*Usp28*$^{F/F}$;Nestin-Cre animals survived past postnatal day 21. FOXJ1+ ependymal cells could readily be identified in the lateral ventricles of *Plk4*$^{F/F}$;*Usp28*$^{F/F}$;Nestin-Cre brains. However, these cells lacked CEP164+ basal bodies and were devoid of motile cilia **(Fig S2D)**. Taken together, these data show that PLK4 is required for centriole amplification in multiciliated ependymal cells *in vitro* and *in vivo*.

PLK4 is required for centriole amplification in mTECs

In mouse trachea epithelial cells (mTECs) centriole amplification is classified into six stages (Zhao et al. 2013). mTECs begin with two parent centrioles (Stage I) that amplify centrioles together with deuterosomes (Stage II). Deuterosomes enlarge and are encircled by multiple procentrioles in a flower-like arrangement (Stage III). Procentrioles elongate (Stage IV) and are detached from deuterosomes and parent centrioles (Stage V). Finally, centrioles dock at the apical membrane and initiate the assembly of muliticilia (Stage VI). To test the requirement of PLK4 for centriole amplification in mTECs, we isolated mTECs from *Plk4*$^{F/F}$;Rosa26-Cre^{ERT2} animals or littermate *Plk4*$^{F/+}$;Rosa26-Cre^{ERT2} controls (hereafter *Plk4*$^{F/F}$;*Cre*^{ERT2} and *Plk4*$^{F/+}$;*Cre*^{ERT2}). Cre recombination was induced *in vitro* with 4OHT 2 days before exposure to an Air Liquid Interface (ALI) and cells were analyzed at various timepoints thereafter **(Fig 3A)**.

Comparable fractions of *Plk4*$^{F/F}$;*Cre*^{ERT2} and *Plk4*$^{F/+}$;*Cre*^{ERT2} mTECs expressed FOXJ1 at ALI 7 and ALI 21 and formed deuterosomes at ALI 3 and ALI 21 **(Fig 3B,C)**. Similar to ependymal cells, CEP152 was recruited to deuterosomes in both *Plk4*$^{F/F}$;*Cre*^{ERT2} and control mTECs **(Fig S3A)**. The percentage of cells with deuterosomes decreased from ~25% at ALI 3 to ~5% at ALI 21 in both control and *PLK4*$^{F/F}$;*Cre*^{ERT2} mTECs **(Fig 3C)**. These data show that mTECs lacking PLK4 undergo similar transitions to cells that amplify centrioles: first recruiting CEP152 to deuterosomes and later degrading/disassembling deuterosomes.

In control mTECs, PLK4 localized to deuterosomes during the early stages of centriole amplification. Deuterosomal levels of PLK4 declined after centriole disengagement, and weak PLK4 staining was retained on disengaged centrioles **(Fig S3B)**. 55% of control

bioRxiv preprint doi: https://doi.org/10.1101/2022.06.06.494981; this version posted June 7, 2022. The copyright holder for this preprint (which was not certified by peer review) is the author/funder, who has granted bioRxiv a license to display the preprint in perpetuity. It is made available under a CC-BY 4.0 International license.

mTECs exhibited PLK4 staining on deuterosomes at ALI 3, reflecting the percentage of DEUP1+ cells in the early stages of amplification. However, PLK4 was only present on deuterosomes in 15% of *Plk4*$^{F/F}$;*Cre*^{ERT2} mTECs at ALI 3 **(Fig 3D,E**). Consistent with the loss of PLK4, the deuterosomal recruitment of the cartwheel proteins STIL and SAS6 was impaired in *Plk4*$^{F/F}$;*Cre*^{ERT2} mTECs **(Fig 3F,G; Fig S3C,D)**. Moreover, while 40% of control mTECs formed multiple cilia, only 4% of *PLK4*$^{F/F}$;*Cre*^{ERT2} mTECs contained CEP164+ basal bodies and nucleated motile cilia by ALI 7 **(Fig 3H,I).**

To ensure that centriole amplification and ciliogenesis were blocked and not simply delayed by the loss of PLK4, we analyzed mTECs at ALI 21. Although ~25% of both control and *PLK4*$^{F/F}$;*Cre*^{ERT2} mTECs expressed FOXJ1 **(Fig 3B)**, fewer than 5% of *PLK4*$^{F/F}$;*Cre*^{ERT2} mTECs underwent centriole amplification at ALI 21 **(Fig 3J,K)**. The small fraction of *Plk4*$^{F/F}$;*Cre*^{ERT2} cells that underwent centriole amplification are likely to have escaped Cre-mediated recombination and consequently express PLK4 at normal levels. We conclude that PLK4 is also required for centriole amplification in mTECs.

mTECs that fail centriole amplification accumulate assemblies of centriole components

Control mTECs frequently formed irregularly shaped assemblies of the distal centriole protein Centrin at the early stages of centriole amplification. However, these structures were mostly absent in fully differentiated multiciliated cells **(Fig S4A)**. By contrast, 4OHT-treated *Plk4*$^{F/F}$;*Cre*^{ERT2} cells that failed centriole amplification formed large filamentous assemblies of Centrin (hereafter PLK4 knockout) **(Fig 4A,B)**. To analyze these assemblies in greater detail, we performed expansion microscopy on control and PLK4 knockout mTECs at ALI 3. In control mTECs, amplified procentrioles were stained with acetylated-α-tubulin to mark the centriole microtube wall, and Centrin which resides in the lumen of the centriole **(Fig 4C)**. In PLK4 knockout mTECs, acetylated-α-tubulin and Centrin marked the parent centrioles (**Fig 4D**, arrows) and the filamentous Centrin assemblies. Consistent with the observations in ependymal cells, procentrioles were not observed in mTECs lacking PLK4.

bioRxiv preprint doi: https://doi.org/10.1101/2022.06.06.494981; this version posted June 7, 2022. The copyright holder for this preprint (which was not certified by peer review) is the author/funder, who has granted bioRxiv a license to display the preprint in perpetuity. It is made available under a CC-BY 4.0 International license.

To investigate the physical properties of the Centrin assemblies, we performed Fluorescence Recovery after Photobleaching (FRAP) in PLK4 knockout and control mTECs expressing Centrin-GFP. While Centrin-GFP recovered by 23% over 10 mins at the amplified centrioles of control mTECs, recovery was limited to 10% in the filamentous assemblies formed in mTECs lacking PLK4 **(Fig S4B,C)**.

We examined the localization of several other centriole and PCM proteins in mTECs lacking PLK4. The proximal centriole protein CEP135 formed large spherical assemblies in PLK4 knockout mTECs. These assemblies were distinct from the filamentous assemblies of Centrin observed in mTECs that fail centriole amplification (**Fig 4B)**. The distal centriole protein Centrobin, the distal appendage component CEP164 and the PCM protein γTubulin also formed ectopic assemblies in mTECs lacking PLK4 **(Fig 4E-G)**. However, the centriole cartwheel components STIL and SAS6, and the PCM component CDK5RAP2 did not form detectable assemblies in *PLK4*$^{F/F}$;*Cre*^{ERT2} mTECs **(Fig 3G, Fig S3C, Fig S4D)**.

To determine whether the assemblies of centriole proteins are caused by a failure of centriole amplification, we examined the effect of knocking out the centriole component SAS4 in mTECs. At ALI 7 ~35% of control *Sas4*$^{F/+}$;*Cre*^{ERT2} mTECs were multiciliated, while ~18% of *Sas4*$^{F/F}$;*Cre*^{ERT2} mTECs formed multiciliated cells **(Fig S4E,F)**. At the same time point, 15% of *Sas4*$^{F/F}$;*Cre*^{ERT2} mTECs displayed filamentous assemblies of Centrin and spherical assemblies of CEP135, a penetrance similar to that observed in mTECs lacking PLK4 **(Fig S4G)**. These data suggest that the elevated expression of centriole proteins in mTECs drives the formation of assemblies of specific centriole components when centriole amplification is prevented.

Evaluating centrinone as a tool to inhibit PLK4 kinase activity in mouse MCCs

We next investigated the requirement of PLK4 kinase activity for centriole amplification in MCCs. A previous study reported that treatment with 1.5 μM of the PLK4 inhibitor centrinone failed to block procentriole production in ependymal cells (Zhao et al. 2019). Given that this concentration of centrinone may be insufficient to fully inhibit PLK4 in

bioRxiv preprint doi: https://doi.org/10.1101/2022.06.06.494981; this version posted June 7, 2022. The copyright holder for this preprint (which was not certified by peer review) is the author/funder, who has granted bioRxiv a license to display the preprint in perpetuity. It is made available under a CC-BY 4.0 International license.

MCCs, we treated differentiating ependymal cells with a broad range of centrinone concentrations (1-10 μM). After 5 days, PLK4 abundance on deuterosomes was measured as a readout of PLK4 inhibition (Holland et al. 2010). The levels of PLK4 progressively increased in ependymal cells treated with ≥ 2.5 μM centrinone **(Fig S5A)**. At doses above 2.5 μM we also observed a progressive decline in the fraction of MBB and disengagement (D) phase cells and an increase in the fraction of cells in amplification (A) or growth (G) phase **(Fig S5B,C)**. Moreover, cells that reached MBB phase in the presence of 5 μM or 10 μM centrinone contained fewer centrioles than controls **(Fig S5D,E)**. There was a significant impact on cell health and viability at doses of centrinone above 10 μM which prevented us from exploring whether higher doses of centrinone could fully block centriole amplification.

Previous work shows that treatment with 1 μM of centrinone does not perturb centriole amplification in mTECs (Nanjundappa et al. 2019). To define if higher doses of centrinone can suppress centriole assembly, we treated differentiating mTECs with 10 μM centrinone. 10 μM centrinone did not change the percentage of multiciliated mTECs at ALI 7, or the number of centrioles made per cell **(Fig S5F-H)**. However, there was no increase in PLK4 abundance on deuterosomes in mTECs treated with 1-10 μM of centrinone, a hallmark of kinase inactivation in cycling cells **(Fig S5I,J)**. This suggests that either PLK4 kinase activity is dispensable for centriole amplification in mTECs or centrinone is unable to effectively inhibit PLK4 in this cell type.

PLK4 kinase activity is required for centriole assembly in MCCs

Our experiments with centrinone revealed limitations of using small molecule inhibitors to probe the role of PLK4 kinase activity in multiciliated cells. To overcome these drawbacks, we created a conditional kinase-dead allele of PLK4 in mice (*Plk4*^{cKD}). The *Plk4*^{cKD} allele was generated by knockin of a D154A kinase-dead mutation into exon 5. A *LoxP*-STOP-*LoxP* cassette was inserted into intron 4 of the *Plk4* gene to ensure that the *Plk4*^{cKD} allele was only expressed following Cre-mediated recombination. As a control, we also created an analogous conditional wild-type allele of *Plk4* that lacked the kinase inactivating mutation (*Plk4*^{cWT}) **(Fig S6A)**.

bioRxiv preprint doi: https://doi.org/10.1101/2022.06.06.494981; this version posted June 7, 2022. The copyright holder for this preprint (which was not certified by peer review) is the author/funder, who has granted bioRxiv a license to display the preprint in perpetuity. It is made available under a CC-BY 4.0 International license.

To explore the requirement for PLK4 kinase activity, we infected *Plk4*$^{cWT/F}$ and *Plk4*$^{cKD/F}$ ependymal cells with AAV-Cre. Following Cre expression, the *Plk4* floxed allele is inactivated and the conditional wild type or kinase-dead allele is expressed. PLK4 was present on the deuterosomes of almost all Cre+ *Plk4*$^{cKD/F}$ ependymal cells (**Fig 5A**). Moreover, PLK4 abundance on deuterosomes was ~3-fold higher in Cre+ *Plk4*$^{cKD/F}$ ependymal cells (**Fig 5B-D**), and STIL staining was absent from deuterosomes (**Fig S6C,D**). This is consistent with observations in cycling cells that showed PLK4 kinase activity is required to recruit STIL to the site of procentriole assembly on parent centrioles (Moyer et al. 2015). 60% of Cre+ *Plk4*$^{cWT/F}$ ependymal cells formed multicilia. However, Cre+ *Plk4*$^{cKD/F}$ ependymal cells failed to undergo centriole amplification and produced very few multiciliated cells (**Fig 5D,E**).

To determine if PLK4 kinase activity is essential for multiciliogenesis in mTECs, we isolated mTECs from *Plk4*$^{cWT/F}$*;Cre*^{ERT2} and *Plk4*$^{cKD/F}$*;Cre*^{ERT2} animals and treated them with 4OHT to induce Cre-mediated recombination before differentiation. While Cre had no impact on centriole amplification in *Plk4*$^{cWT/F}$*;Cre*^{ERT2} mTECs, *Plk4*$^{cKD/F}$*;Cre*^{ERT2} mTECs possessed large Centrin filaments and few procentrioles **(Fig S7B)**. Moreover, while 50% of *Plk4*$^{cWT/F}$*;Cre*^{ERT2} mTECs nucleated multicilia, less than 5% of *Plk4*$^{cKD/F}$*;Cre*^{ERT2} mTECs contained basal bodies and nucleated motile cilia by ALI 7 (**Fig S7A,B**). These data show that PLK4 kinase activity is required to drive centriole biogenesis in multiciliated cells.

We noted that differentiating ependymal cells and mTECs expressing kinase-dead PLK4 had irregular-shaped deuterosomes that were larger but fewer in number **(Fig 5F,G, Fig S7C-E)**. In contrast, deuterosome size and number were unchanged in differentiating ependymal cells and mTECs that lacked PLK4 **(Fig 5F,G, Fig S7C-E).** These data suggest that the accumulation of kinase-inactive PLK4 on the surface of deuterosomes changes the properties of these organelles.

Centriole amplification is required for apical surface area expansion in mTECs

bioRxiv preprint doi: https://doi.org/10.1101/2022.06.06.494981; this version posted June 7, 2022. The copyright holder for this preprint (which was not certified by peer review) is the author/funder, who has granted bioRxiv a license to display the preprint in perpetuity. It is made available under a CC-BY 4.0 International license.

Previous work has shown that centriole number scales proportionally with the apical surface area of muticiliated *Xenopus* epidermal cells and mTECs (Nanjundappa et al. 2019; Kulkarni et al. 2021). To investigate what drives this scaling phenomenon, we examined apical surface area in muticiliated cells that fail to undergo centriole amplification. The surface area of control mTECs progressively increased throughout differentiation as procentrioles are seeded, elongate, and disengage from deuterosomes **(Fig 6A,B)**.

We next examined apical surface area in PLK4 or SAS4 knockout mTECs that failed centriole amplification and contained filamentous assemblies of Centrin. As a control, we also quantified cells in the same culture that escaped Cre-mediated recombination and underwent centriole amplification. At ALI 3, when most muticiliated cells are in the early stages of differentiation, the average apical surface area was similar in control and PLK4 knockout mTECs **(Fig 6C,D)**. However, while control mTECs increased their average apical surface area from 90 to 159 μm^2 from ALI 3 to ALI 7, PLK4 and SAS4 knockout mTECs failed to undergo this expansion. Notably, apical surface area expansion was still observed in MBB phase cells that escaped Cre-recombination **(Fig 6C,E,F)**. These data show that centriole amplification plays a critical role in promoting apical membrane expansion in differentiating mTECs.

bioRxiv preprint doi: https://doi.org/10.1101/2022.06.06.494981; this version posted June 7, 2022. The copyright holder for this preprint (which was not certified by peer review) is the author/funder, who has granted bioRxiv a license to display the preprint in perpetuity. It is made available under a CC-BY 4.0 International license.

Discussion

MCCs transcriptionally upregulate many of the proteins required for centriole duplication in cycling cells, but whether the molecular mechanisms driving centriole assembly are the same in cycling cells and MCCs remains unclear (Hoh et al. 2012; Revinski et al. 2018; Zaragosi et al. 2020). In this manuscript, we employed a genetic approach to test the impact of inactivating the *Plk4* gene or kinase activity in differentiating mouse MCCs. Conditional knockout of PLK4 blocked procentriole assembly and multiciliogenesis without preventing MCC differentiation. Although the PLK4 receptor CEP152 was recruited to deuterosomes and parent centrioles in MCCs lacking PLK4, the cartwheel proteins STIL and SAS6 were not, demonstrating that PLK4 plays a crucial role in the earliest stages of centriole amplification in MCCs. These results conflict with prior work that observed a delay in centriole assembly in MCCs that were depleted of PLK4 using an shRNA (Nanjundappa et al. 2019). The most likely explanation for this discrepancy is that shRNA-mediated depletion of PLK4 failed to achieve a sufficient level of target depletion required to block centriole assembly. Together, our data show the centriolar and deuterosomal pathways of centriole biogenesis in MCCs have a striking resemblance to the established centriole assembly pathway of cycling cells.

While high doses of the PLK4 inhibitor centrinone reduced centriole production in ependymal multiciliated cells, this was not the case in mTECs. Similarly, a previous study also reported that there was no decrease in centriole number in mTECs treated with centrinone (Nanjundappa et al. 2019). These data could be interpreted to suggest that PLK4 kinase activity is dispensable for centriole amplification, at least in mTECs (Nanjundappa et al. 2019). However, the doses of centrinone used may not fully inhibit PLK4 activity in mTECs, possibly because of the expression of multidrug-resistant transporters that pump drugs out of mTECs (Florea et al. 2001). To address this limitation, we developed a strategy to conditionally ablate PLK4 kinase activity using genetic tools that enable specific and more complete PLK4 inhibition. We show that selectively ablating PLK4 kinase activity leads to a failure of centriole amplification in mTECs and ependymal cells, thereby phenocopying the loss of PLK4 protein.

bioRxiv preprint doi: https://doi.org/10.1101/2022.06.06.494981; this version posted June 7, 2022. The copyright holder for this preprint (which was not certified by peer review) is the author/funder, who has granted bioRxiv a license to display the preprint in perpetuity. It is made available under a CC-BY 4.0 International license.

Multiciliated cells lacking PLK4 kinase activity possessed fewer deuterosomes that were larger in size. Since deuterosomes are unaffected in MCCs lacking PLK4, we speculate that deuterosomes loaded with kinase-inactive PLK4 undergo fusion events that are driven by the self-assembly properties of PLK4 (Montenegro Gouveia et al. 2018; Yamamoto and Kitagawa 2018; Park et al. 2019).

Centriole amplification in MCCs occurs within a cloud of PCM and fibrogranular material. Several centriole components are concentrated within the fibrogranular material, and this has been proposed to facilitate the rapid assembly of centrioles in MCCs (Zhao et al. 2021). In the absence of PLK4, or the centriole protein SAS4, multiple centriole, PCM, and distal appendage proteins formed large independent assemblies in mTECs. These assemblies were not observed in multiciliated ependymal cells, which produce ~3 times fewer centrioles than mTECs and likely have lower concentrations of centriole proteins. The high abundance of centriole proteins in differentiating mTECs is likely to drive protein-protein self-interactions that promote the formation of distinct assemblies when centriole amplification is blocked.

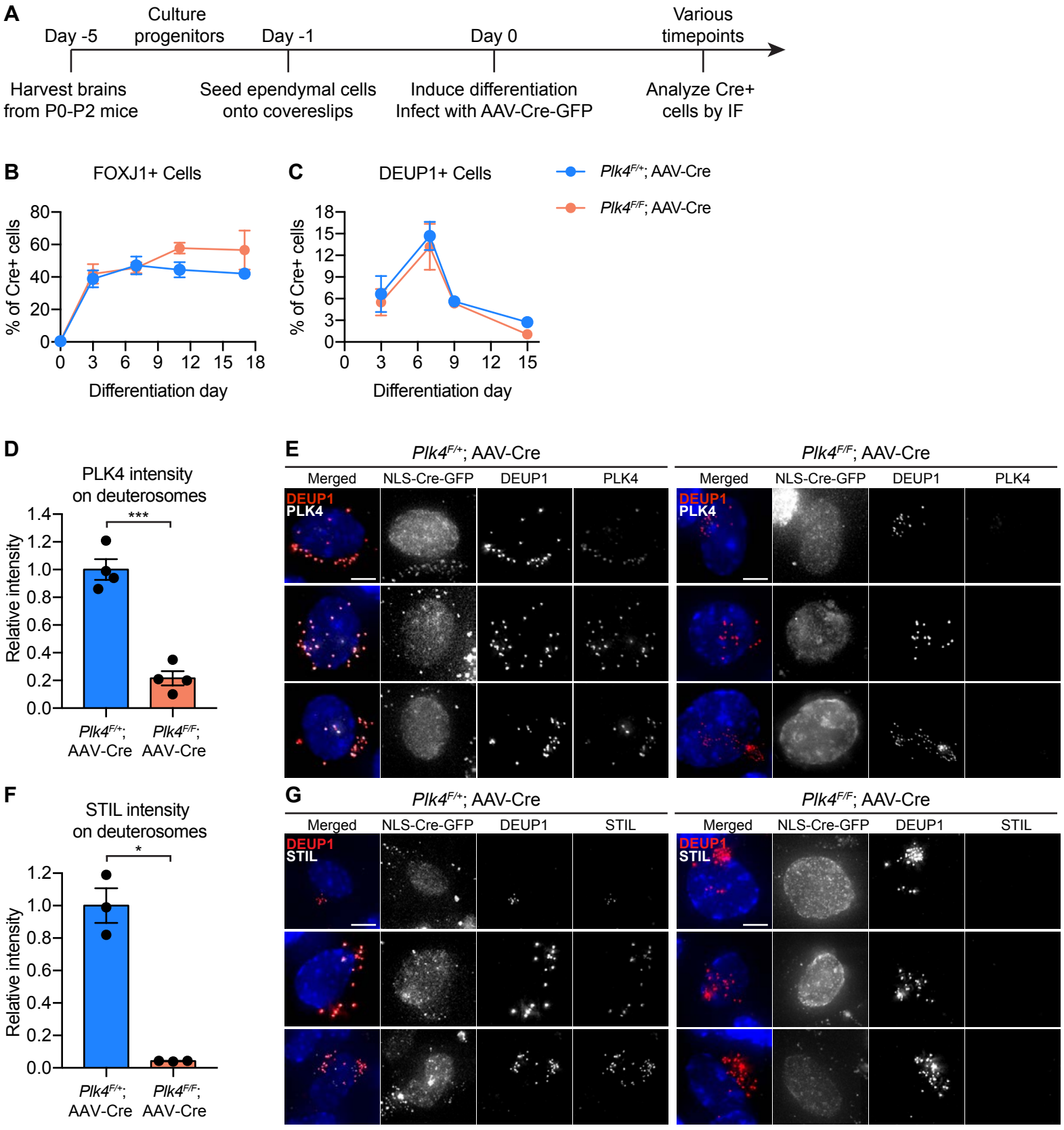
In addition to containing aggregates of centriole proteins, mTECs that fail centriole amplification have a smaller apical surface area. Centriole number has been shown to scale with apical area in multiciliated mTECs and *Xenopus* epithelial cells (Nanjundappa et al. 2019; Kulkarni et al. 2021). Yet, it remains unclear exactly how this scaling relationship is established. Our results show that the apical area of mTECs progressively expands during differentiation, but this fails to occur in cells that lack PLK4 or SAS4 and do not undergo centriole amplification. This suggests that centriole amplification is a central driver of surface area expansion in mammalian multiciliated cells. In *Xenopus* epithelial cells, depleting centriole number did not reduce the surface area of MCCs (Kulkarni et al. 2021). However, multiciliated *Xenopus* epithelial cells undergo two waves of centriole amplification that take place before and after radial intercalation (Kulkarni et al. 2021). By contrast, mammalian MCCs do not radially intercalate and use a single round of centriole production (Al Jord et al. 2014). This suggests that multiple pathways could operate to calibrate centriole numbers with the

bioRxiv preprint doi: https://doi.org/10.1101/2022.06.06.494981; this version posted June 7, 2022. The copyright holder for this preprint (which was not certified by peer review) is the author/funder, who has granted bioRxiv a license to display the preprint in perpetuity. It is made available under a CC-BY 4.0 International license.

MCC apical area. Future studies will be required to define how centriole amplification feeds back to tune the apical surface area of mammalian MCCs.

bioRxiv preprint doi: https://doi.org/10.1101/2022.06.06.494981; this version posted June 7, 2022. The copyright holder for this preprint (which was not certified by peer review) is the author/funder, who has granted bioRxiv a license to display the preprint in perpetuity. It is made available under a CC-BY 4.0 International license.

FIGURE 1



bioRxiv preprint doi: https://doi.org/10.1101/2022.06.06.494981; this version posted June 7, 2022. The copyright holder for this preprint (which was not certified by peer review) is the author/funder, who has granted bioRxiv a license to display the preprint in perpetuity. It is made available under a CC-BY 4.0 International license.

Figure 1: Ependymal cells lacking PLK4 differentiate but fail to recruit STIL to deuterosomes.

(A) Schematic overview of the experiment to recombine the *Plk4*$^{F/F}$ allele in ependymal cells *in vitro*. Ependymal cells were harvested from *Plk4*$^{F/F}$ mice or *Plk4*$^{F/+}$ controls and seeded onto coverslips. On differentiation day 0, the ependymal cells were transduced with AAV-Cre in serum-free media.

(B) Quantification of the percent of FOXJ1-expressing ependymal cells transduced with AAV-Cre-GFP. N = 3-4 brains, n > 300 cells. Two-tailed Welch's t-test.

(C) Quantification of the percent of AAV-Cre-GFP transduced ependymal cells with deuterosomes. Day 0 N = 3, day 7 N = 5, day 9 N = 2, day 15 N = 3; n > 300 cells. Two-tailed Welch's t-test.

(D) Quantification of the intensity of PLK4 on deuterosomes in ependymal cells on differentiation day 7. Cells in all stages of centriole amplification were measured and pooled. N = 4, n $\geq$ 20. Two-tailed Welch's t-test.

(E) Confocal images of *Plk4*$^{F/F}$ or *Plk4*$^{F/+}$ ependymal cells transduced with AAV-Cre-GFP. Cells were stained with DEUP1 to mark deuterosomes (red) and PLK4 (white). Scale bar = 5 μm.

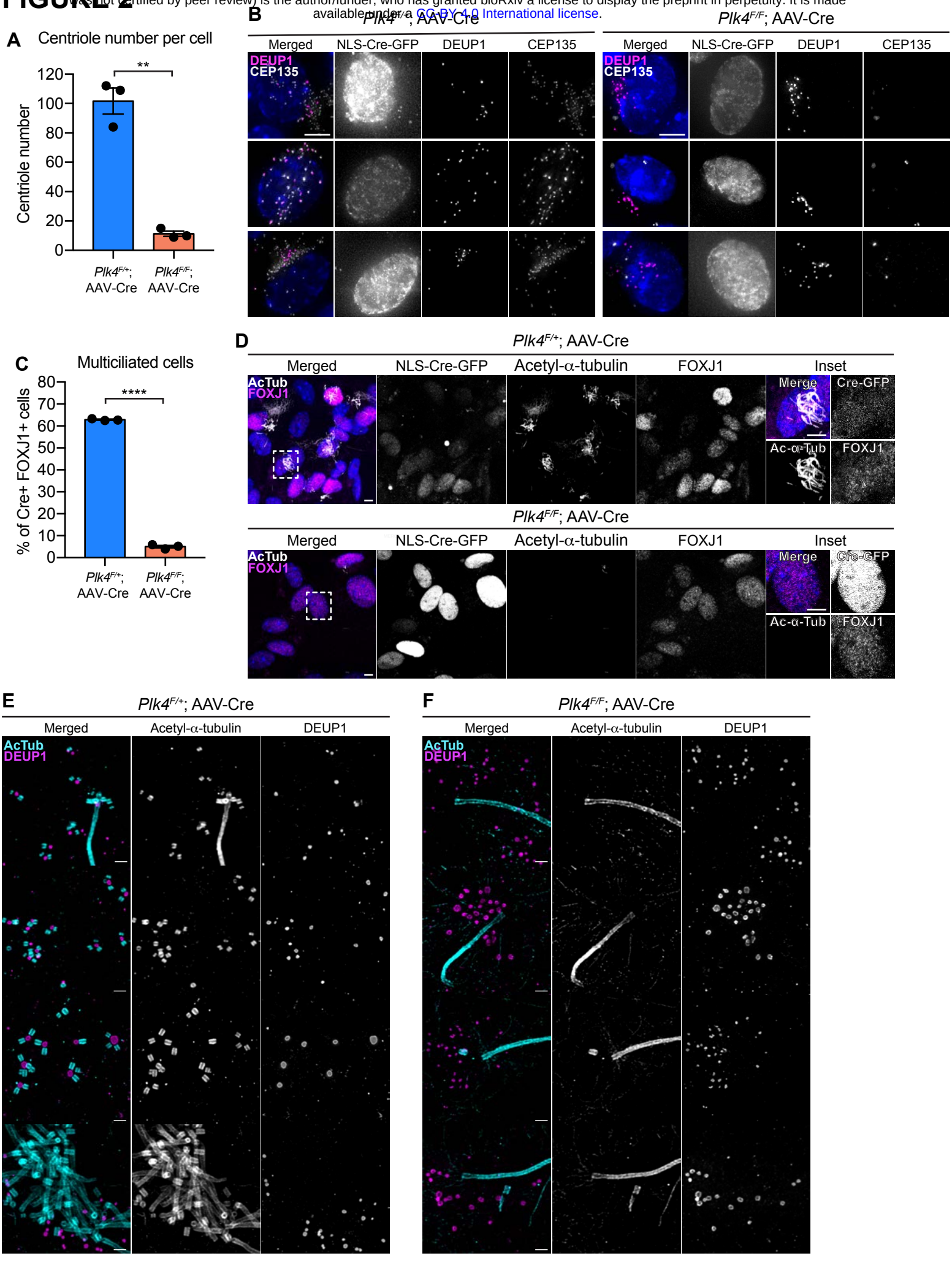
(F) Quantification of the intensity of STIL on deuterosomes in ependymal cells on differentiation day 7. Cells in all stages of centriole amplification were measured and pooled. N = 3, n $\geq$ 30. Two-tailed Welch's t-test.

(G) Confocal images of *Plk4*$^{F/F}$ or *Plk4*$^{F/+}$ ependymal cells transduced with AAV-Cre-GFP. Cells were stained with DEUP1 (red) and STIL (white). Scale bar = 5 μm.

Data information: All data represent the means $\pm$ SEM. *P < 0.05; ***< 0.001 .

bioRxiv preprint doi: https://doi.org/10.1101/2022.06.06.494981; this version posted June 7, 2022. The copyright holder for this preprint (which was not certified by peer review) is the author/funder, who has granted bioRxiv a license to display the preprint in perpetuity. It is made available under a CC-BY 4.0 International license.

FIGURE 2



bioRxiv preprint doi: https://doi.org/10.1101/2022.06.06.494981; this version posted June 7, 2022. The copyright holder for this preprint (which was not certified by peer review) is the author/funder, who has granted bioRxiv a license to display the preprint in perpetuity. It is made available under a CC-BY 4.0 International license.

Figure 2: Loss of PLK4 blocks centriole assembly in ependymal cells.

(A) Quantification of the number of centrioles per cell in disengagement (D) phase. *Plk4*$^{F/F}$ or *Plk4*$^{F/+}$ ependymal cells transduced with AAV-Cre-GFP were analyzed at differentiation day 7-8. N = 3, n $\geq$ 20. Two-tailed Welch's t-test.

(B) Images of *Plk4*$^{F/F}$ or *Plk4*$^{F/+}$ ependymal cells transduced with AAV-Cre-GFP. Cells were stained with DEUP1 (magenta) and CEP135 to mark centrioles (white). Scale bar = 5 μm.

(C) Quantification of the percent of FOXJ1+ *Plk4*$^{F/F}$ or *Plk4*$^{F/+}$ ependymal cells transduced with AAV-Cre-GFP that have multiple motile cilia at differentiation day 12. N = 3, n > 300. Two-tailed Welch's t-test.

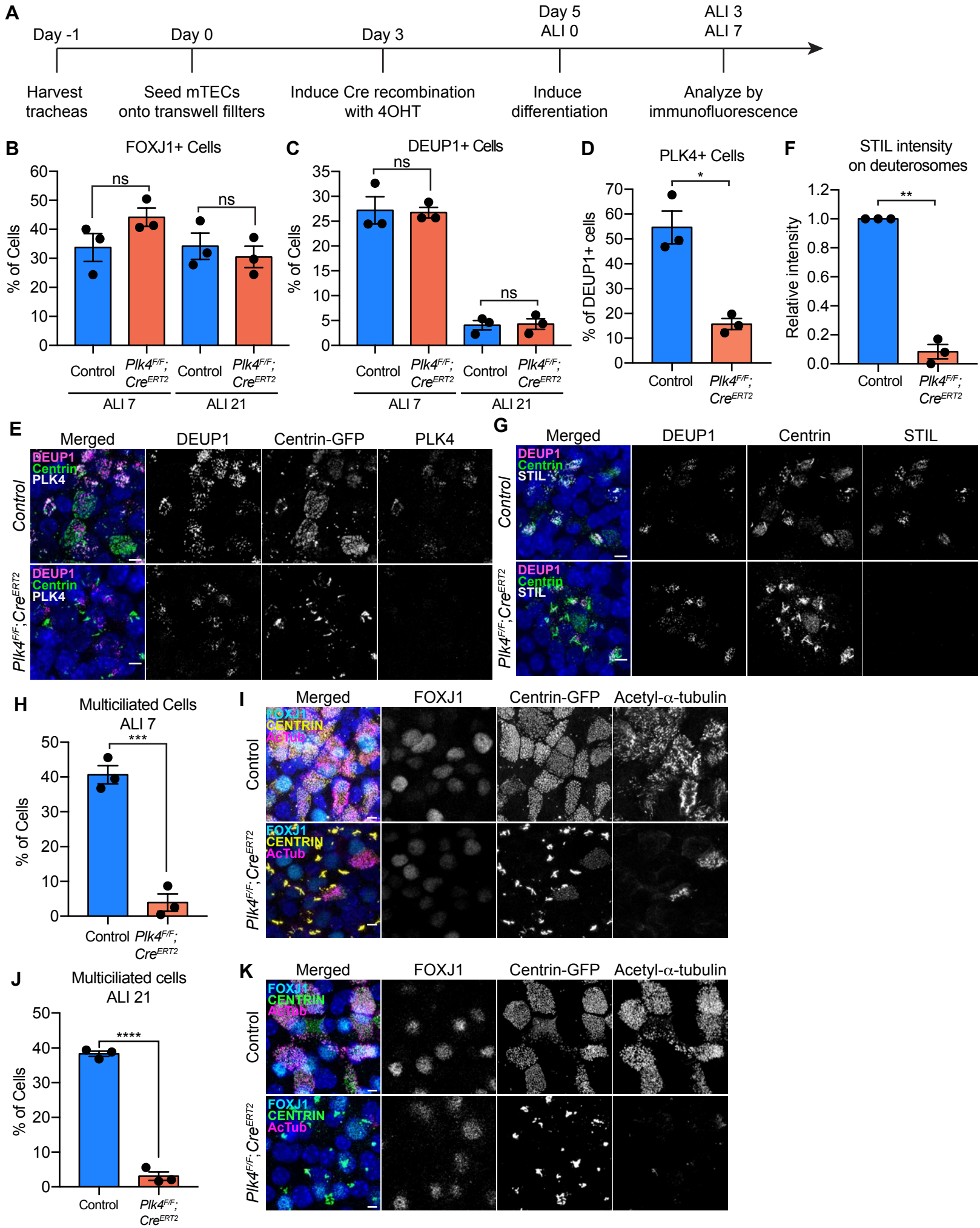
(D) Confocal images of *Plk4*$^{F/F}$ or *Plk4*$^{F/+}$ ependymal cells transduced with AAV-Cre-GFP. Cells were stained with antibodies against FOXJ1 (magenta) and acetylated-α-tubulin (white). Scale bar = 5 μm.

(E-F) Expansion microscopy of *Plk4*$^{F/F}$ or *Plk4*$^{F/+}$ ependymal cells transduced with AAV-Cre-GFP. Cells were stained with acetylated-α-tubulin (cyan) and DEUP1 (magenta). Scale bar = 0.5 μM.

Data information: All data represent the means $\pm$ SEM. **P < 0.01; ****< 0.0001.

bioRxiv preprint doi: https://doi.org/10.1101/2022.06.06.494981; this version posted June 7, 2022. The copyright holder for this preprint (which was not certified by peer review) is the author/funder, who has granted bioRxiv a license to display the preprint in perpetuity. It is made available under a CC-BY 4.0 International license.

FIGURE 3



bioRxiv preprint doi: https://doi.org/10.1101/2022.06.06.494981; this version posted June 7, 2022. The copyright holder for this preprint (which was not certified by peer review) is the author/funder, who has granted bioRxiv a license to display the preprint in perpetuity. It is made available under a CC-BY 4.0 International license.

Figure 3: PLK4 promotes centriole assembly in mTECs.

(A) Schematic of the experimental design to genetically deplete PLK4 in mTECs. *Plk4*$^{F/F}$;*Cre*^{ERT2} tracheal epithelial cells were seeded onto collagen-coated transwell filters and allowed to proliferate until confluence (Day 3). At this point Cre-mediated recombination of the *Plk4*$^{F/F}$ allele was induced by the addition of 4OHT to the media. 2 days later, the mTECs were exposed to ALI to initiate differentiation.

(B) Quantification of the percent of control or *Plk4*$^{F/F}$;*Cre*^{ERT2} mTECs expressing FOXJ1 at ALI 7 and ALI 21. N = 3, n > 500. Two-tailed Welch's t-test.

(C) Quantification of the percent of control or *Plk4*$^{F/F}$;*Cre*^{ERT2} mTECs with deuterosomes at ALI 7 and ALI 21. N = 3, n > 500. Two-tailed Welch's t-test.

(D) Quantification of the percent of control or *Plk4*$^{F/F}$;*Cre*^{ERT2} mTECs that express PLK4 at ALI 3. N = 3, n > 500. Two-tailed Welch's t-test.

(E) Confocal images of control and *Plk4*$^{F/F}$;*Cre*^{ERT2} mTECs at ALI 3. Cells were expressing centrin-GFP and stained with DEUP1 (magenta) and PLK4 (white). Scale bar = 5 μm.

(F) Quantification of the intensity of STIL on deuterosomes in control or *Plk4*$^{F/F}$;*Cre*^{ERT2} mTECs at ALI 3. Cells in all stages of centriole amplification were measured and pooled. N = 3, n > 500. Two-tailed Welch's t-test.

(G) Confocal images of control and *Plk4*$^{F/F}$;*Cre*^{ERT2} mTECs at ALI 3. Cells were expressing centrin-GFP and stained with DEUP1 (magenta) and STIL (white). Scale bar = 5 μm.

(H) Quantification of multiciliated mTECs at ALI 7. N = 3, n > 500. Two-tailed Welch's t-test.

(I) Confocal images of control and *Plk4*$^{F/F}$;*Cre*^{ERT2} mTECs at ALI 7. Cells were expressing centrin-GFP (yellow) and stained with FOXJ1 (cyan) and acetylated-α-tubulin (magenta). Scale bar = 5 μm.

(J) Quantification of multiciliated mTECs at ALI 21. N = 3, n > 500. Two-tailed Welch's t-test.

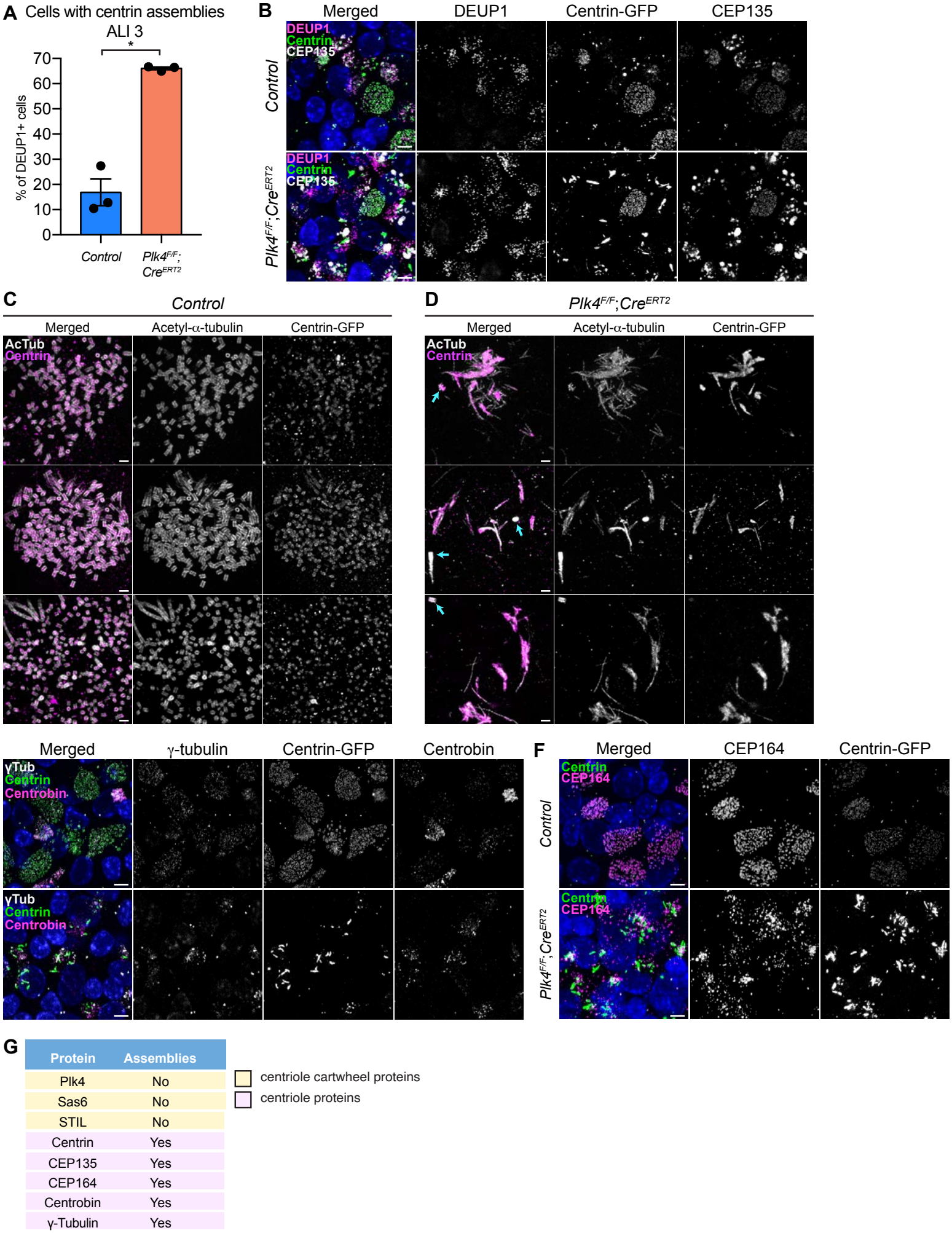
(K) Confocal images of control and *Plk4*$^{F/F}$;*Cre*^{ERT2} mTECs at ALI 21. Cells were expressing centrin-GFP (green) and stained with FOXJ1 (cyan) and acetylated-α-tubulin (magenta). Scale bar = 5 μm.

bioRxiv preprint doi: https://doi.org/10.1101/2022.06.06.494981; this version posted June 7, 2022. The copyright holder for this preprint (which was not certified by peer review) is the author/funder, who has granted bioRxiv a license to display the preprint in perpetuity. It is made available under a CC-BY 4.0 International license.

Data information: All data represent the means ± SEM. *P < 0.05; **< 0.01; ***< 0.001; ****< 0.0001 and not significant indicates P > 0.05.

bioRxiv preprint doi: https://doi.org/10.1101/2022.06.06.494981; this version posted June 7, 2022. The copyright holder for this preprint (which was not certified by peer review) is the author/funder, who has granted bioRxiv a license to display the preprint in perpetuity. It is made available under a CC-BY 4.0 International license.

FIGURE 4



G

Protein	Assemblies
Plk4	No
Sas6	No
STIL	No
Centrin	Yes
CEP135	Yes
CEP164	Yes
Centrobin	Yes
γ-Tubulin	Yes

centriole cartwheel proteins
centriole proteins

bioRxiv preprint doi: https://doi.org/10.1101/2022.06.06.494981; this version posted June 7, 2022. The copyright holder for this preprint (which was not certified by peer review) is the author/funder, who has granted bioRxiv a license to display the preprint in perpetuity. It is made available under a CC-BY 4.0 International license.

Figure 4: mTECs that fail centriole amplification form aberrant assemblies of centriole proteins.

(A) Quantification of the percent of control and *Plk4*$^{F/F}$;*Cre*^{ERT2} mTECs with centrin aggregates at ALI 3. N = 3, n > 150. Two-tailed Welch's t-test.

(B) Confocal images of control and *Plk4*$^{F/F}$;*Cre*^{ERT2} mTECs at ALI 3. Cells were expressing centrin-GFP and stained with DEUP1 (magenta) and CEP135 (white). Scale bar = 5 μm.

(C-D) Confocal images of control and *Plk4*$^{F/F}$;*Cre*^{ERT2} mTECs expanded by ultrastructure expansion microscopy (UExM). Cells were stained with antibodies against acetylated-α-tubulin (white) and GFP (magenta). Blue arrows indicate parent centrioles. Scale bar = 0.5 μM.

(E) Confocal images of control and *Plk4*$^{F/F}$;*Cre*^{ERT2} mTECs. Cells were expressing centrin-GFP and stained with antibodies against γ-tubulin (white) and Centrobin (magenta). Scale bar = 5 μm.

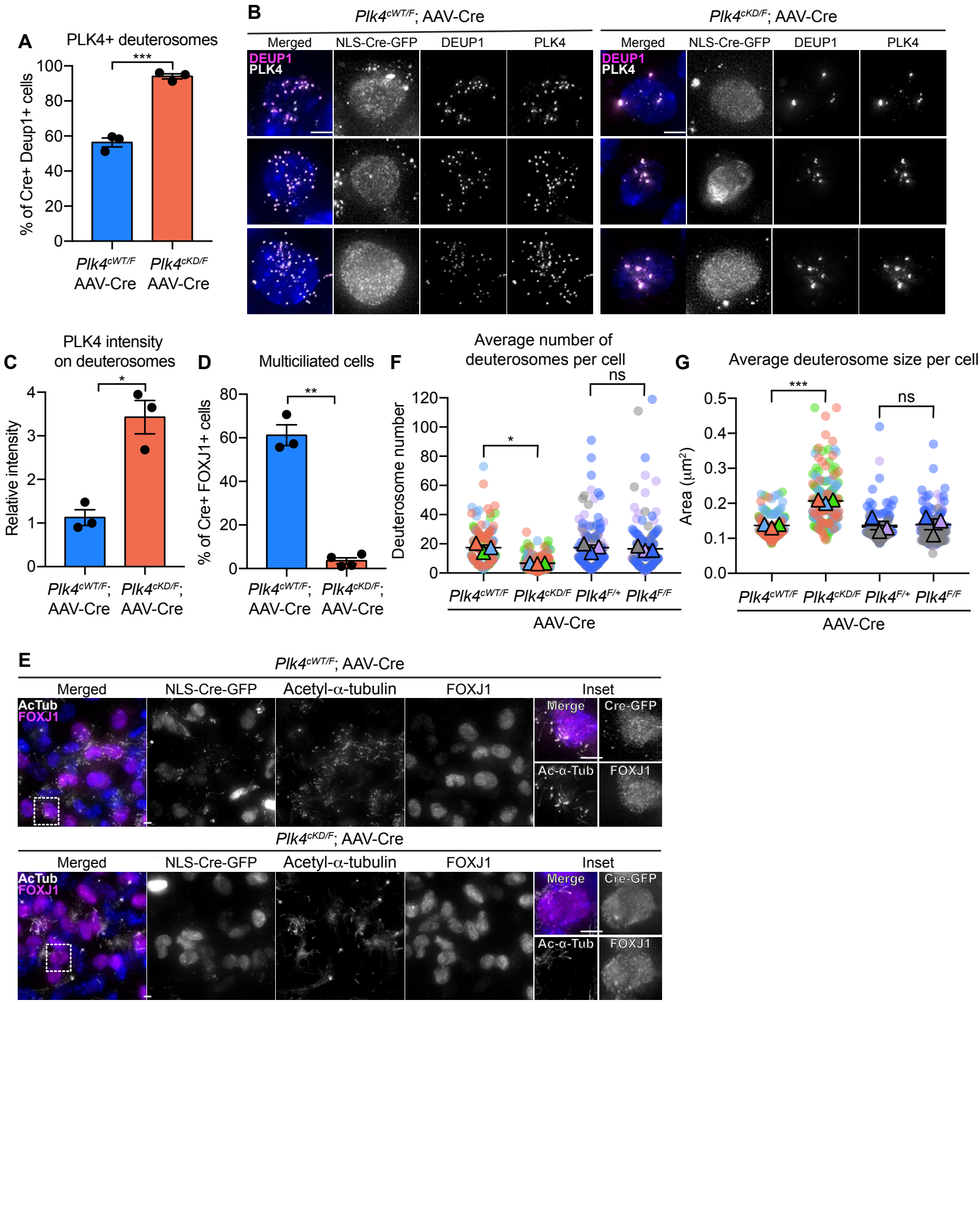
(F) Confocal images of control and *Plk4*$^{F/F}$;*Cre*^{ERT2} mTECs. Cells were expressing centrin-GFP and stained with an antibody against CEP164 (magenta). Scale bar = 5 μm.

(G) Table showing which of the centriole proteins form assemblies in *Plk4*$^{F/F}$;*Cre*^{ERT2} mTECs.

Data information: All data represent the means ± SEM. *P < 0.05.

bioRxiv preprint doi: https://doi.org/10.1101/2022.06.06.494981; this version posted June 7, 2022. The copyright holder for this preprint (which was not certified by peer review) is the author/funder, who has granted bioRxiv a license to display the preprint in perpetuity. It is made available under a CC-BY 4.0 International license.

FIGURE 5



bioRxiv preprint doi: https://doi.org/10.1101/2022.06.06.494981; this version posted June 7, 2022. The copyright holder for this preprint (which was not certified by peer review) is the author/funder, who has granted bioRxiv a license to display the preprint in perpetuity. It is made available under a CC-BY 4.0 International license.

Figure 5: Plk4 kinase activity is critical for centriole amplification in MCCs.

(A) Percent of AAV-Cre transduced ependymal cells with PLK4 on deuterosomes. N = 3, n > 70. Two-tailed Welch's t-test.

(B) Representative images of AAV-Cre transduced *Plk4*$^{cWT/F}$ and *Plk4*$^{cKD/F}$ ependymal cells stained with DEUP1 (magenta) and PLK4 (white). Scale bar = 5 μm.

(C) Quantification of the intensity of PLK4 on deuterosomes in ependymal cells on differentiation day 5. Cells in all stages of centriole amplification were measured and pooled. N = 3, n ≥ 50. Two-tailed Welch's t-test.

(D) Quantification of the percent of FOXJ1+ *Plk4*$^{cWT/F}$ or *Plk4*$^{cKD/F}$ ependymal cells transduced with AAV-Cre-GFP that have multiple motile cilia at differentiation day 12. N = 3, n ≥ 100. Two-tailed Welch's t-test.

(E) Confocal images of *Plk4*$^{cWT/F}$ or *Plk4*$^{cKD/F}$ ependymal cells transduced with AAV-Cre-GFP at differentiation day 12. Cells were stained with antibodies against FOXJ1 (magenta) and acetylated-α-tubulin (white). Scale bar = 5 μm.

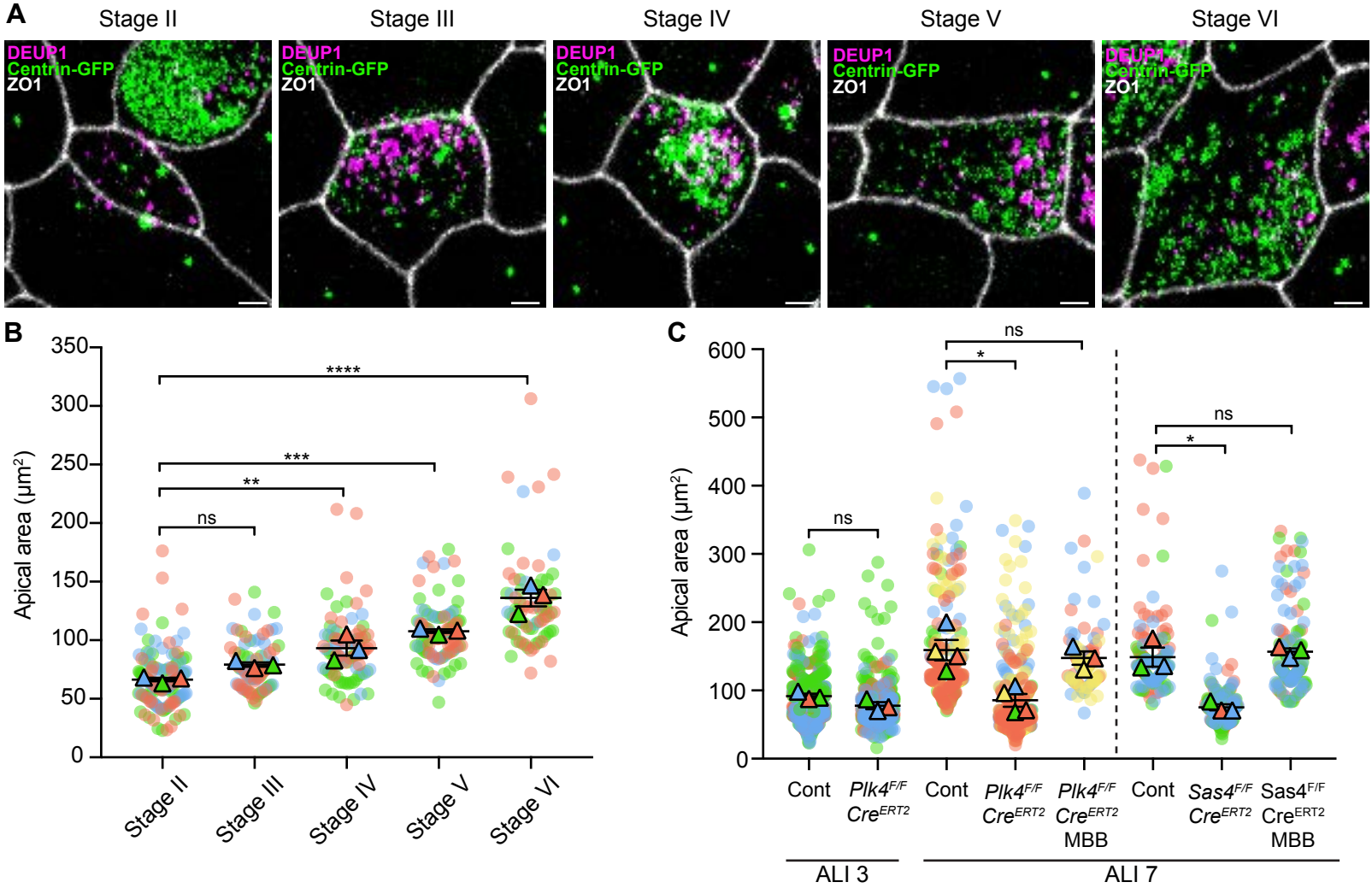
(F) Quantification of the average number of deuterosomes per cell in AAV-Cre transduced *Plk4*$^{cWT/F}$, *Plk4*$^{cKD/F}$, *Plk4*$^{F/+}$ or *Plk4*$^{F/F}$ ependymal cells. N = 3, n ≥ 50. Two-tailed Welch's t-test.

(G) Quantification of the average deuterosome size per cell in AAV-Cre transduced *Plk4*$^{cWT/F}$, *Plk4*$^{cKD/F}$, *Plk4*$^{F/+}$ or *Plk4*$^{F/F}$ ependymal cells. N = 3, n ≥ 50. Two-tailed Welch's t-test.

Data information: All data represent the means ± SEM. *P < 0.05; **< 0.01; ***< 0.001; and not significant indicates P > 0.05.

bioRxiv preprint doi: https://doi.org/10.1101/2022.06.06.494981; this version posted June 7, 2022. The copyright holder for this preprint (which was not certified by peer review) is the author/funder, who has granted bioRxiv a license to display the preprint in perpetuity. It is made available under a CC-BY 4.0 International license.

FIGURE 6



bioRxiv preprint doi: https://doi.org/10.1101/2022.06.06.494981; this version posted June 7, 2022. The copyright holder for this preprint (which was not certified by peer review) is the author/funder, who has granted bioRxiv a license to display the preprint in perpetuity. It is made available under a CC-BY 4.0 International license.

Figure 6: Centriole amplification promotes apical surface area expansion in mTECs.

(A) Representative confocal images of control mTECs in stages II-VI of centriole amplification. Cells were expressing centrin-GFP and stained with antibodies against DEUP1 (magenta) and ZO1 (white). Scale bar = 2 μm.

(B) Graph of the apical area of control mTECs (marked with ZO1) at ALI 3 at different stages of centriole amplification. Circles represent individual cells and triangles represent the average per biological replicate. N = 3, n ≥ 20. One-way ANOVA with *post hoc* analysis.

(C) Graph of the apical area of control, *Plk4*$^{F/F}$;*Cre*^{ERT2} and *Sas4*$^{F/F}$;*Cre*^{ERT2} mTECs at ALI 3 and ALI 7. The area across all stages of centriole amplification was pooled per condition. MBB phase cells that presumably escaped Cre-mediated recombination serve as an internal control. Circles represent individual cells and triangles represent the average per biological replicate. N ≥ 3, n ≥ 50. Two-tailed Welch's t-test (ALI 3). One-way ANOVA with *post hoc* analysis (ALI 7).

(D) Representative confocal images of control and *Plk4*$^{F/F}$;*Cre*^{ERT2} mTECs at ALI 3. Cells were expressing centrin-GFP and stained with antibodies against DEUP1 (magenta) and ZO1 (white). Scale bar = 5 μm.

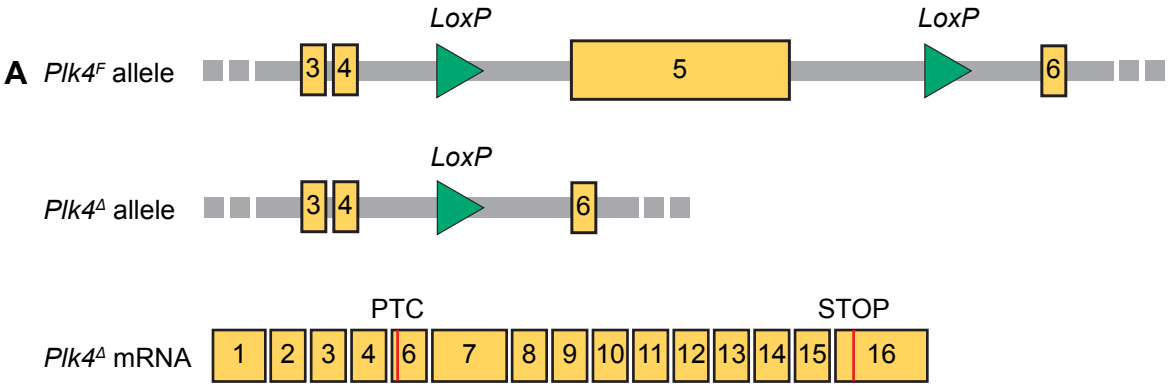
(E) Representative confocal images of control mTECs at ALI 7. *Plk4*$^{F/+}$;*Cre*^{ERT2} cells were expressing centrin-GFP and stained with antibodies against FOXJ1 (magenta) and ZO1 (white). *Sas4*$^{F/F}$ cells were stained with antibodies against centrin (green) and ZO1 (white). Scale bar = 5 μm.

(F) Representative confocal images of *Plk4*$^{F/F}$;*Cre*^{ERT2} and *Sas4*$^{F/F}$;*Cre*^{ERT2} mTECs at ALI 7. *Plk4*$^{F/F}$;*Cre*^{ERT2} cells were expressing centrin-GFP and stained with antibodies against FOXJ1 (magenta) and ZO1 (white). *Sas4*$^{F/F}$;*Cre*^{ERT2} cells were stained with antibodies against centrin (green) and ZO1 (white). MBB phase cells that presumably escaped Cre-mediated recombination are marked with an *. Scale bar = 5 μm.

Data information: All data represent the means ± SEM. *P < 0.05; **< 0.01; ***< 0.001; ****< 0.0001 and not significant indicates P > 0.05.

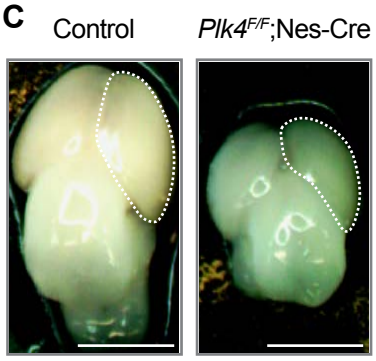
bioRxiv preprint doi: https://doi.org/10.1101/2022.06.06.494981; this version posted June 7, 2022. The copyright holder for this preprint (which was not certified by peer review) is the author/funder, who has granted bioRxiv a license to display the preprint in perpetuity. It is made available under a CC-BY 4.0 International license.

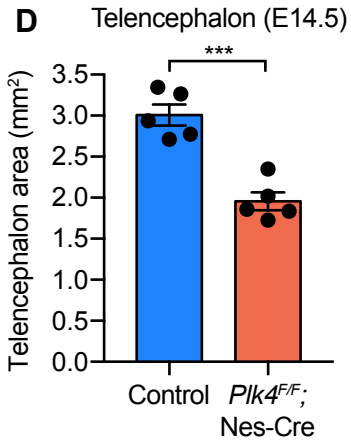
FIGURE S1

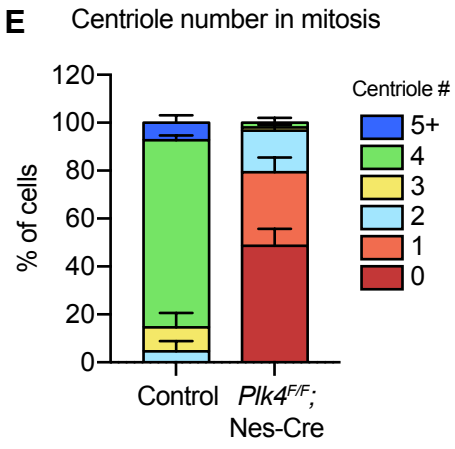


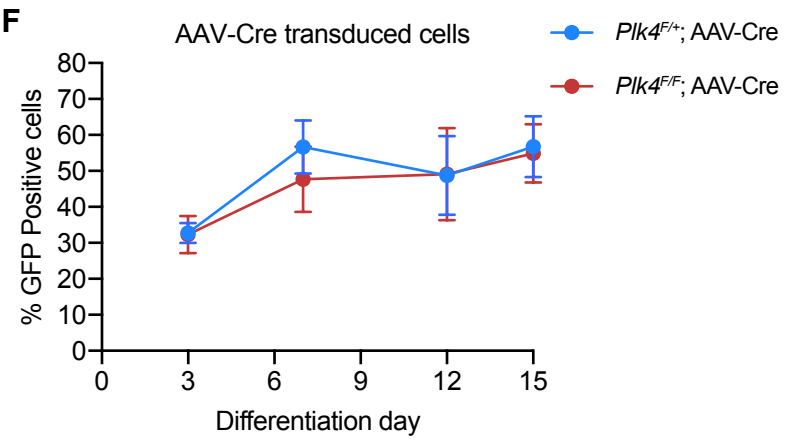
B

Mating	$Plk4^{F/\Delta}$ x $Plk4^{F/\Delta}$
# pups	28
$Plk4^{F/F}$	11 (39%)
$Plk4^{F/\Delta}$	17 (61%)
$Plk4^{\Delta/\Delta}$	0 (0%)









bioRxiv preprint doi: https://doi.org/10.1101/2022.06.06.494981; this version posted June 7, 2022. The copyright holder for this preprint (which was not certified by peer review) is the author/funder, who has granted bioRxiv a license to display the preprint in perpetuity. It is made available under a CC-BY 4.0 International license.

Figure S1: Knockout of PLK4 leads to centriole loss in neural progenitor cells.

(A) Diagram of the *Plk4*^{F} allele showing *LoxP* sites surrounding exon 5 (top). Diagram of the *Plk4*$^{\Delta}$ allele following Cre-mediated recombination (middle). Diagram of the mRNA product created from the *Plk4*$^{\Delta}$ allele showing the premature termination codon (PTC) in exon 6 (bottom).

(B) Frequency of progeny generated from intercrosses of *Plk4*$^{F/\Delta}$ mice. N = 28.

(C) Representative whole-mount images of control and *Plk4*$^{F/F}$;Nestin-Cre brains at E14.5. Scale bar = 0.2 cm.

(D) Telencephalon area of control and *Plk4*$^{F/F}$;Nestin-Cre brains at E14.5. N = 5; Two-tailed Welch's t-test.

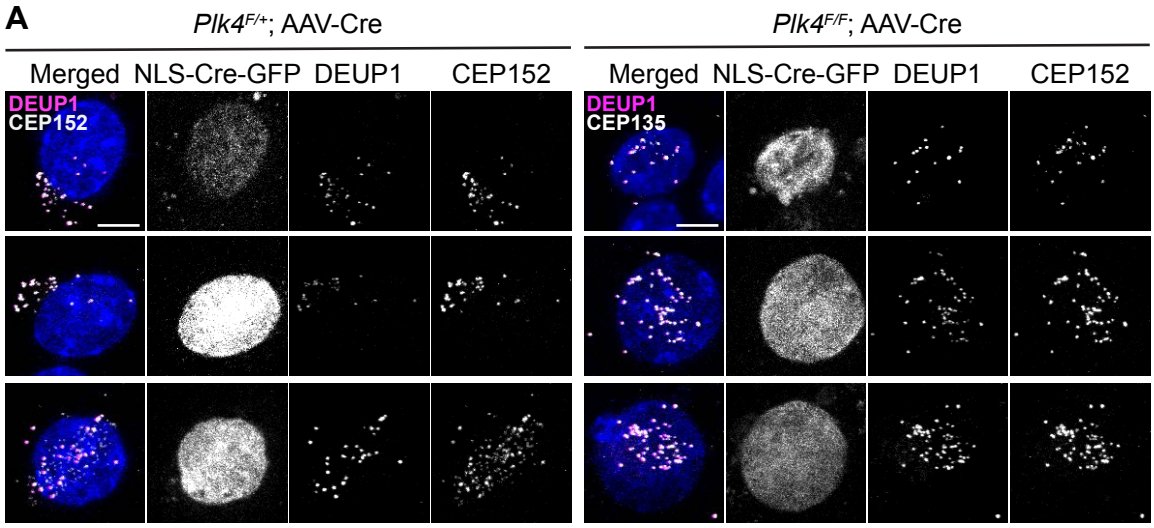
(E) Graph showing centriole number per cell in mitotic neural progenitor cells from control and *Plk4*$^{F/F}$;Nestin-Cre brains at E14.5. N = 3. Two-tailed Welch's t-test.

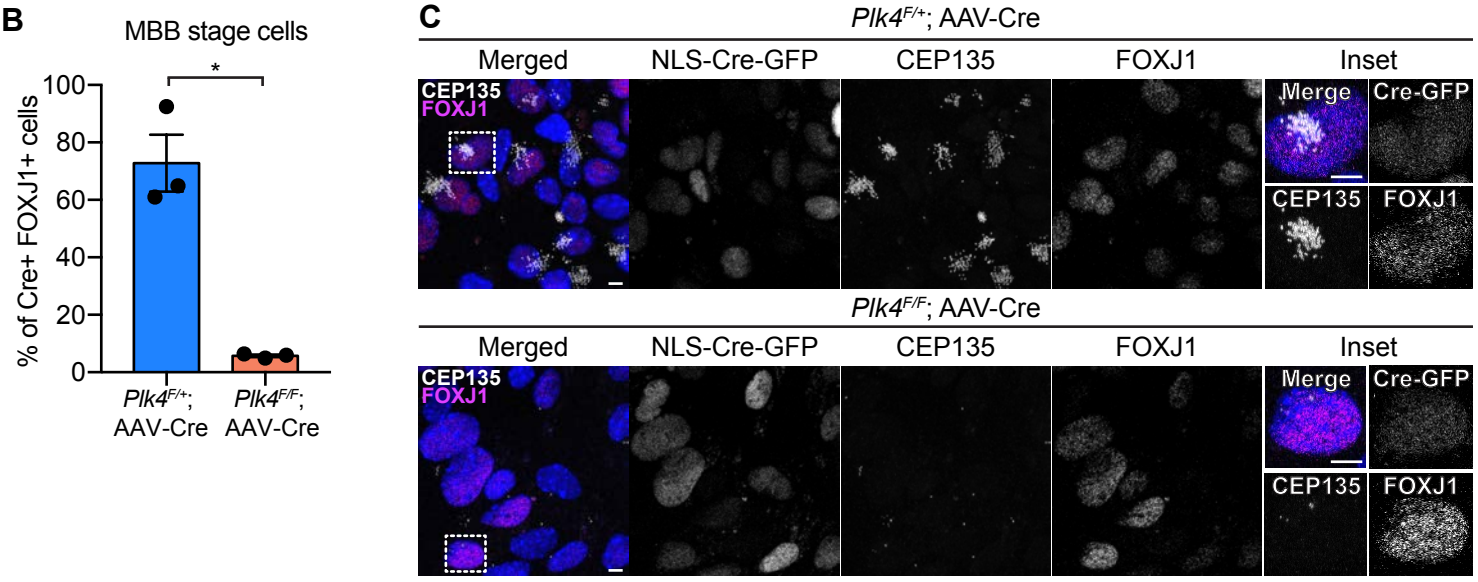
(F) Quantification of the percent of ependymal cells expressing GFP following transduction with AAV-Cre-GFP. N $\geq$ 3, n > 300. Two-tailed Welch's t-test.

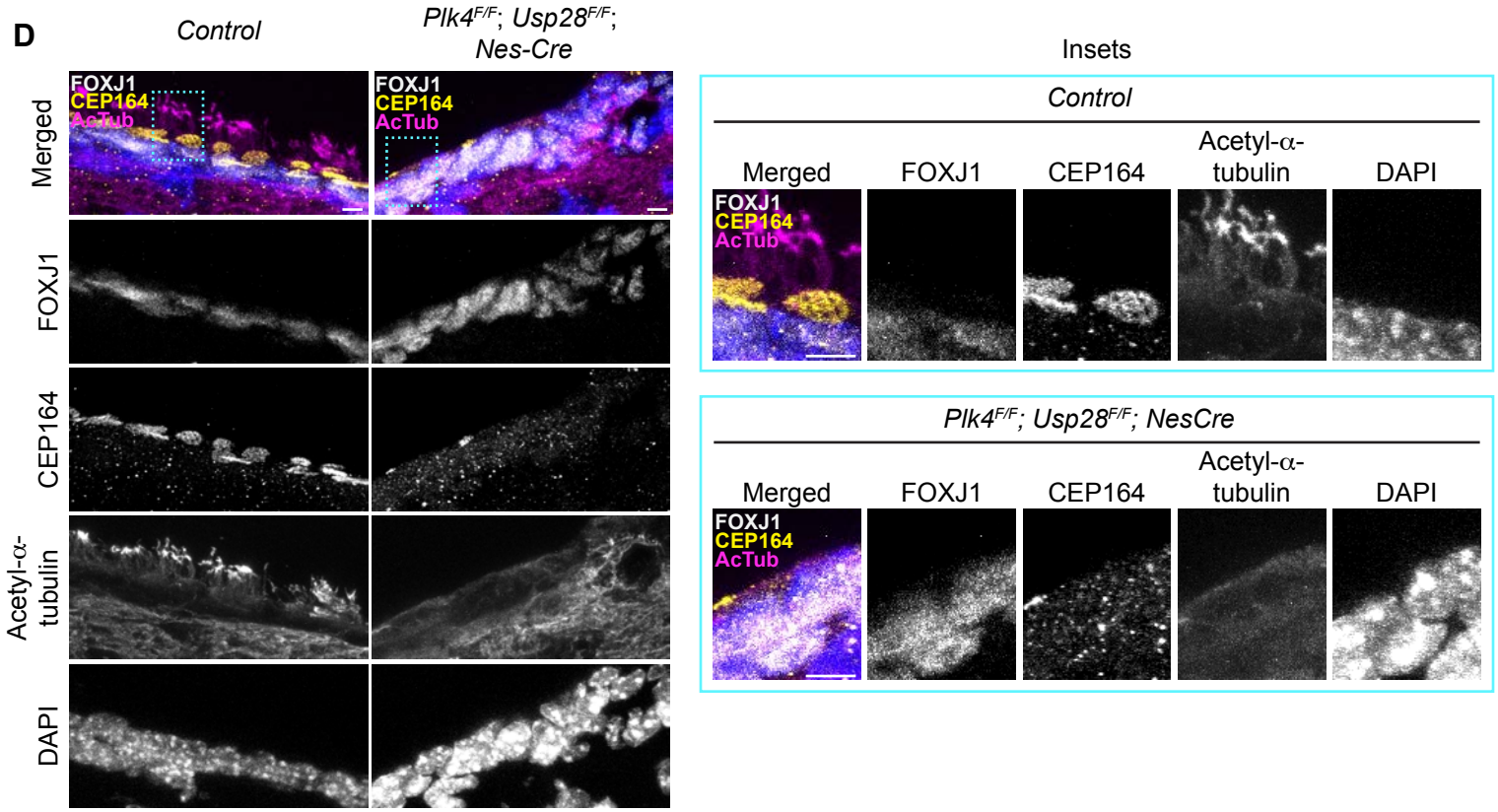
Data information: All data represent the means $\pm$ SEM. ***P < 0.001.

bioRxiv preprint doi: https://doi.org/10.1101/2022.06.06.494981; this version posted June 7, 2022. The copyright holder for this preprint (which was not certified by peer review) is the author/funder, who has granted bioRxiv a license to display the preprint in perpetuity. It is made available under a CC-BY 4.0 International license.

FIGURE S2







bioRxiv preprint doi: https://doi.org/10.1101/2022.06.06.494981; this version posted June 7, 2022. The copyright holder for this preprint (which was not certified by peer review) is the author/funder, who has granted bioRxiv a license to display the preprint in perpetuity. It is made available under a CC-BY 4.0 International license.

Figure S2: Ependymal cells lacking PLK4 recruit CEP152 but fail centriole amplification.

(A) Representative images of *Plk4*$^{F/F}$ or *Plk4*$^{F/+}$ ependymal cells transduced with AAV-Cre-GFP. Cells were stained with antibodies against DEUP1 (white) and CEP152 (magenta). Scale bar = 5 μm.

(B) Quantification of the percent of AAV-Cre-GFP transduced FOXJ1+ *Plk4*$^{F/F}$ or *Plk4*$^{F/+}$ ependymal cells with amplified centrioles (MBB stage) at differentiation day 11. N = 3, n > 100. Two-tailed Welch's t-test.

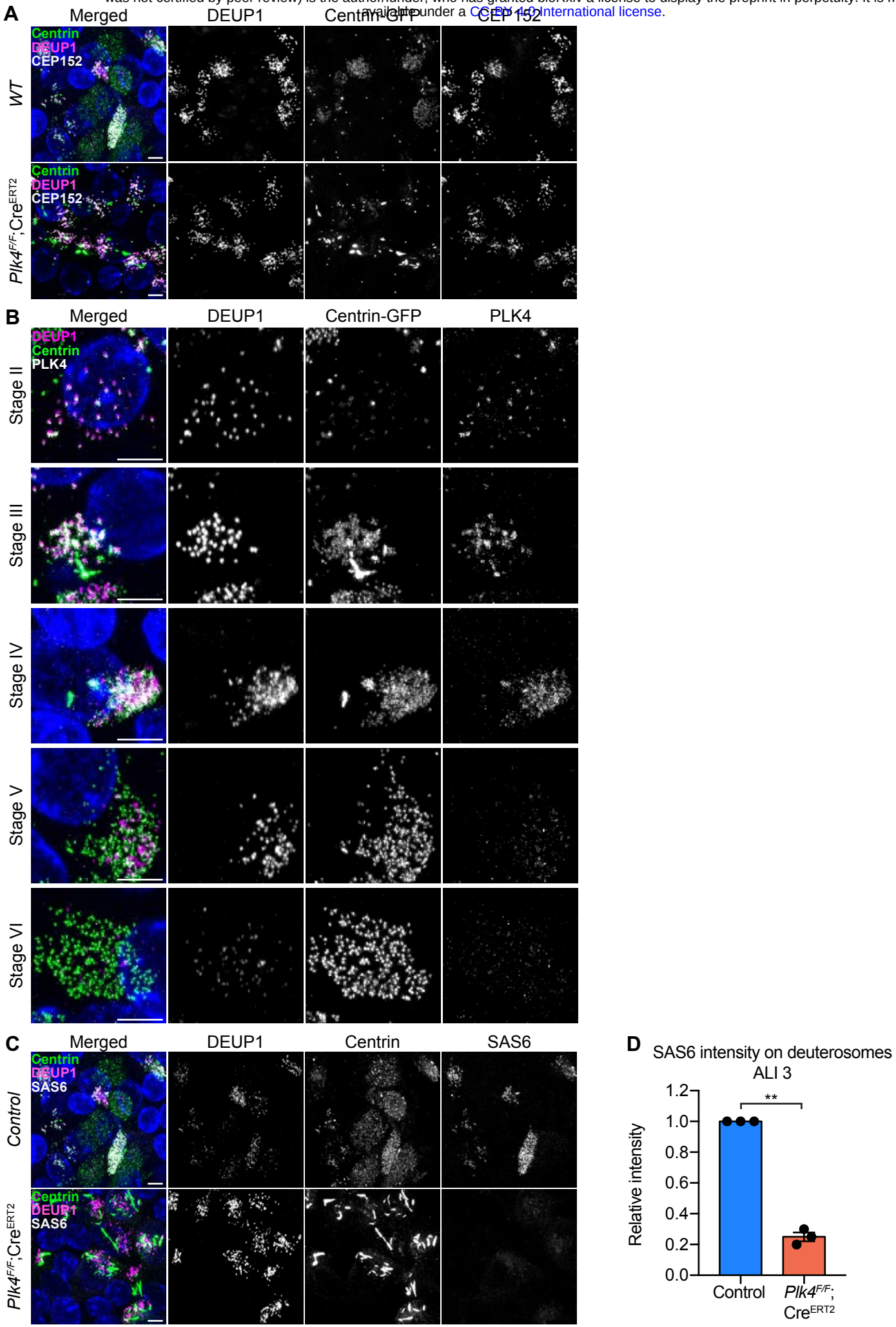
(C) Representative images of *Plk4*$^{F/F}$ or *Plk4*$^{F/+}$ ependymal cells transduced with AAV-Cre-GFP. Cells were stained with antibodies against CEP135 (white) and FOXJ1 (magenta). Scale bar = 5 μm.

(D) Confocal images of the lateral ventricle from control or *Plk4*$^{F/F}$;*Usp28*$^{F/F}$;Nestin-Cre mouse brains at P21. Sections were stained with antibodies against FOXJ1 (white), CEP164 (yellow), and acetylated-α-tubulin (magenta). Scale bar = 5 μm.

Data information: All data represent the means ± SEM. *P < 0.05.

bioRxiv preprint doi: https://doi.org/10.1101/2022.06.06.494981; this version posted June 7, 2022. The copyright holder for this preprint (which was not certified by peer review) is the author/funder, who has granted bioRxiv a license to display the preprint in perpetuity. It is made available under a CC-BY 4.0 International license.

FIGURE S3



bioRxiv preprint doi: https://doi.org/10.1101/2022.06.06.494981; this version posted June 7, 2022. The copyright holder for this preprint (which was not certified by peer review) is the author/funder, who has granted bioRxiv a license to display the preprint in perpetuity. It is made available under a CC-BY 4.0 International license.

Figure S3: mTECs lacking PLK4 recruit CEP152 but fail centriole amplification.

(A) Representative confocal images of control and *Plk4*$^{F/F}$;*Cre*^{ERT2} mTECs at ALI 3. Cells were expressing Centrin-GFP and stained with antibodies against DEUP1 (magenta) and CEP152 (white). Scale bar = 5 μm.

(B) Representative images of control mTECs in stages II-VI of centriole amplification demonstrating PLK4 localization during differentiation. Cells are expressing centrin-GFP and stained with antibodies against DEUP1 (magenta) and PLK4 (white). Scale bar = 5 μm.

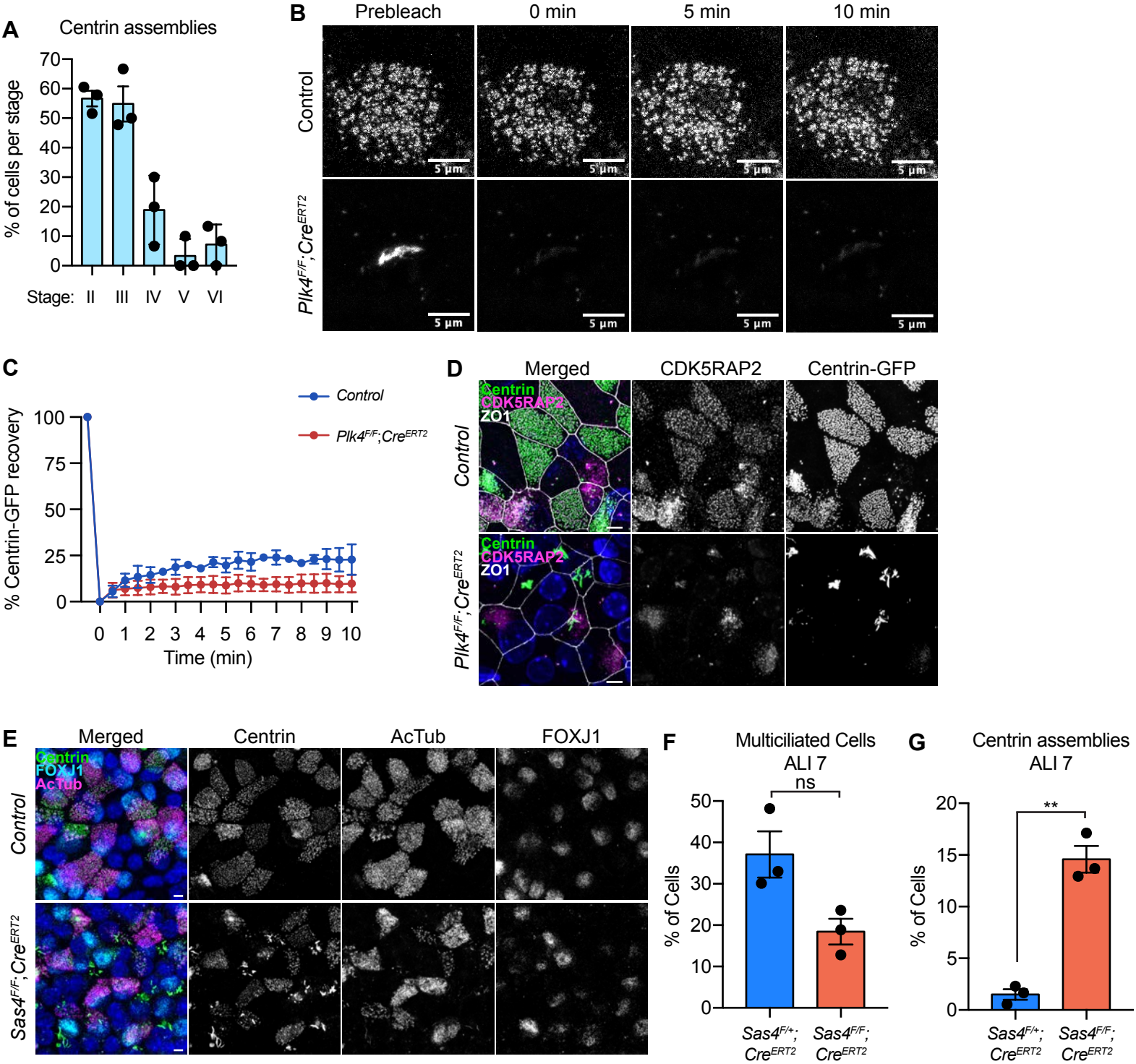
(C) Representative images of control and *Plk4*$^{F/F}$;*Cre*^{ERT2} mTECs at ALI 3 stained with antibodies against DEUP1 (magenta), centrin (green) and SAS6 (white). Scale bar = 5 μm.

(D) Quantification of the average total intensity of SAS6 on deuterosomes per cell in control or *Plk4*$^{F/F}$;*Cre*^{ERT2} mTECs at ALI 3. Cells in all stages of centriole amplification were measured and pooled. N = 3, n > 50. Two-tailed Welch's t-test.

Data information: All data represent the means ± SEM. **P < 0.01.

bioRxiv preprint doi: https://doi.org/10.1101/2022.06.06.494981; this version posted June 7, 2022. The copyright holder for this preprint (which was not certified by peer review) is the author/funder, who has granted bioRxiv a license to display the preprint in perpetuity. It is made available under a CC-BY 4.0 International license.

FIGURE S4



bioRxiv preprint doi: https://doi.org/10.1101/2022.06.06.494981; this version posted June 7, 2022. The copyright holder for this preprint (which was not certified by peer review) is the author/funder, who has granted bioRxiv a license to display the preprint in perpetuity. It is made available under a CC-BY 4.0 International license.

Figure S4: Blocking centriole amplification in mTECs results in assemblies of some centriole proteins.

(A) Graph showing the percent of cells with Centrin aggregates in stages II-VI of centriole amplification in control mTECs at ALI 3. N = 3, n > 50.

(B) Representative images of control and *Plk4*$^{F/F}$;*Cre*^{ERT2} mTECs expressing Centrin-GFP before and at various timepoints after photobleaching.

(C) Quantification of the percent of Centrin-GFP fluorescence recovery after photobleaching in control and *Plk4*$^{F/F}$;*Cre*^{ERT2} mTECs.

(D) Confocal images of control and *Plk4*$^{F/F}$;*Cre*^{ERT2} mTECs at ALI 7 expressing. Cells were centrin-GFP and stained with antibodies against CDK5RAP2 (magenta) and ZO1 (white). Scale bar = 5 μm.

(E) Representative images of control and *Sas4*$^{F/F}$;*Cre*^{ERT2} mTECs at ALI 7. Cells were stained with antibodies against DEUP1 (white), Centrin (green), and CEP135 (magenta). Scale bar = 5 μm.

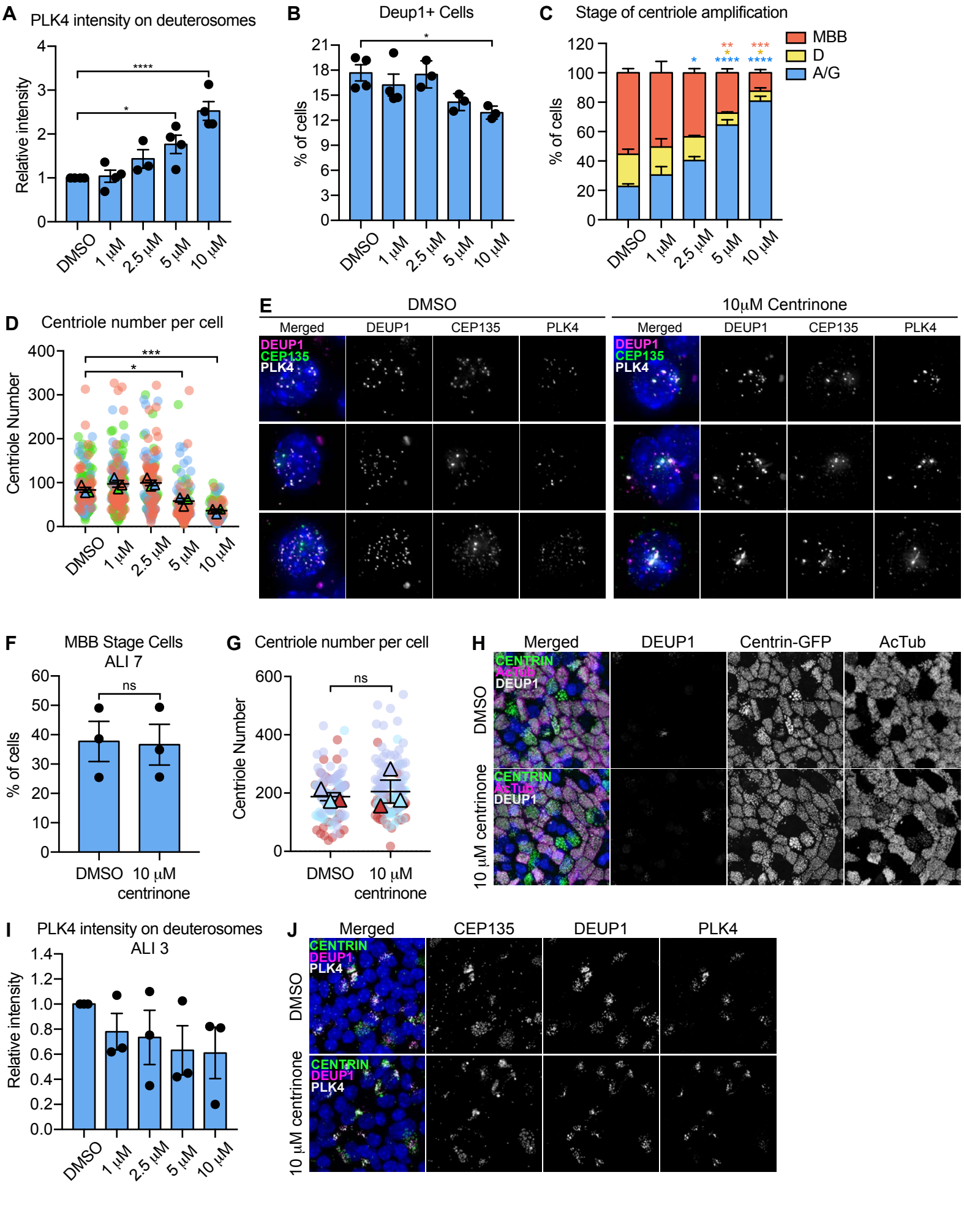
(F) Quantification of the percent of control and *Plk4*$^{F/F}$;*Cre*^{ERT2} mTECs that have multiple motile cilia at ALI 7. N = 3, n > 300. Two-tailed Welch's t-test.

(G) Quantification of the percent of control and *Plk4*$^{F/F}$;*Cre*^{ERT2} mTECs that have centrin aggregates at ALI 7. N = 3, n > 300. Two-tailed Welch's t-test.

Data information: All data represent the means ± SEM. **P < 0.01 and not significant indicates P > 0.05.

bioRxiv preprint doi: https://doi.org/10.1101/2022.06.06.494981; this version posted June 7, 2022. The copyright holder for this preprint (which was not certified by peer review) is the author/funder, who has granted bioRxiv a license to display the preprint in perpetuity. It is made available under a CC-BY 4.0 International license.

FIGURE S5



bioRxiv preprint doi: https://doi.org/10.1101/2022.06.06.494981; this version posted June 7, 2022. The copyright holder for this preprint (which was not certified by peer review) is the author/funder, who has granted bioRxiv a license to display the preprint in perpetuity. It is made available under a CC-BY 4.0 International license.

Figure S5: Inhibition of PLK4 kinase activity with centrinone delays centriole amplification in ependymal cells.

(A) Quantification of the intensity of PLK4 on deuterosomes in ependymal cells treated with DMSO or increasing concentrations of centrinone on differentiation day 5. Cells in all stages of centriole amplification were measured and pooled. $N \geq 3$, $n > 20$. One-way ANOVA with *post hoc* analysis.

(B) Quantification of the percent of ependymal cells with deuterosomes (marked by DEUP1). Cells were treated with DMSO or increasing concentrations of centrinone and analyzed at differentiation day 7. $N \geq 3$, $n > 100$. One-way ANOVA with *post hoc* analysis.

(C) Quantification of the percent of DEUP1+ ependymal cells in A or G stage, D stage, or MBB stage of centriole amplification. Cells were treated with DMSO or one-way ANOVA with *post hoc* analysis.

(D) Quantification of the number of centrioles per cell in disengagement (D) phase. Ependymal cells were treated with DMSO or centrinone and analyzed at differentiation day 7. $N = 3$, $n \geq 17$. One-way ANOVA with *post hoc* analysis.

(E) Representative images of ependymal cells treated with DMSO or 10μM of centrinone. Cells were stained with antibodies against CEP135 (green), DEUP1 (magenta), and PLK4 (white).

(F) Quantification of the percent of MBB stage mTECs at ALI 7 treated with either DMSO or 10μM centrinone. $N = 3$, $n > 300$. Two-tailed Welch's t-test.

(G) Quantification of the number of centrioles per cell in MBB stage mTECs treated with DMSO or 10μM of centrinone at ALI 7. $N = 3$, $n > 50$. Two-tailed Welch's t-test.

(H) Representative confocal images of mTECs treated with DMSO or 10μM of centrinone. Cells were analyzed at ALI 7 and stained with antibodies against Centrin (green), DEUP1 (white), and acetylated-α-tubulin (magenta).

(I) Quantification of the intensity of PLK4 on deuterosomes in mTECs treated with DMSO or increasing concentrations of centrinone at ALI 7. Cells in all stages of centriole amplification were measured and pooled. $N \geq 3$, $n > 50$. One-way ANOVA with *post hoc* analysis.

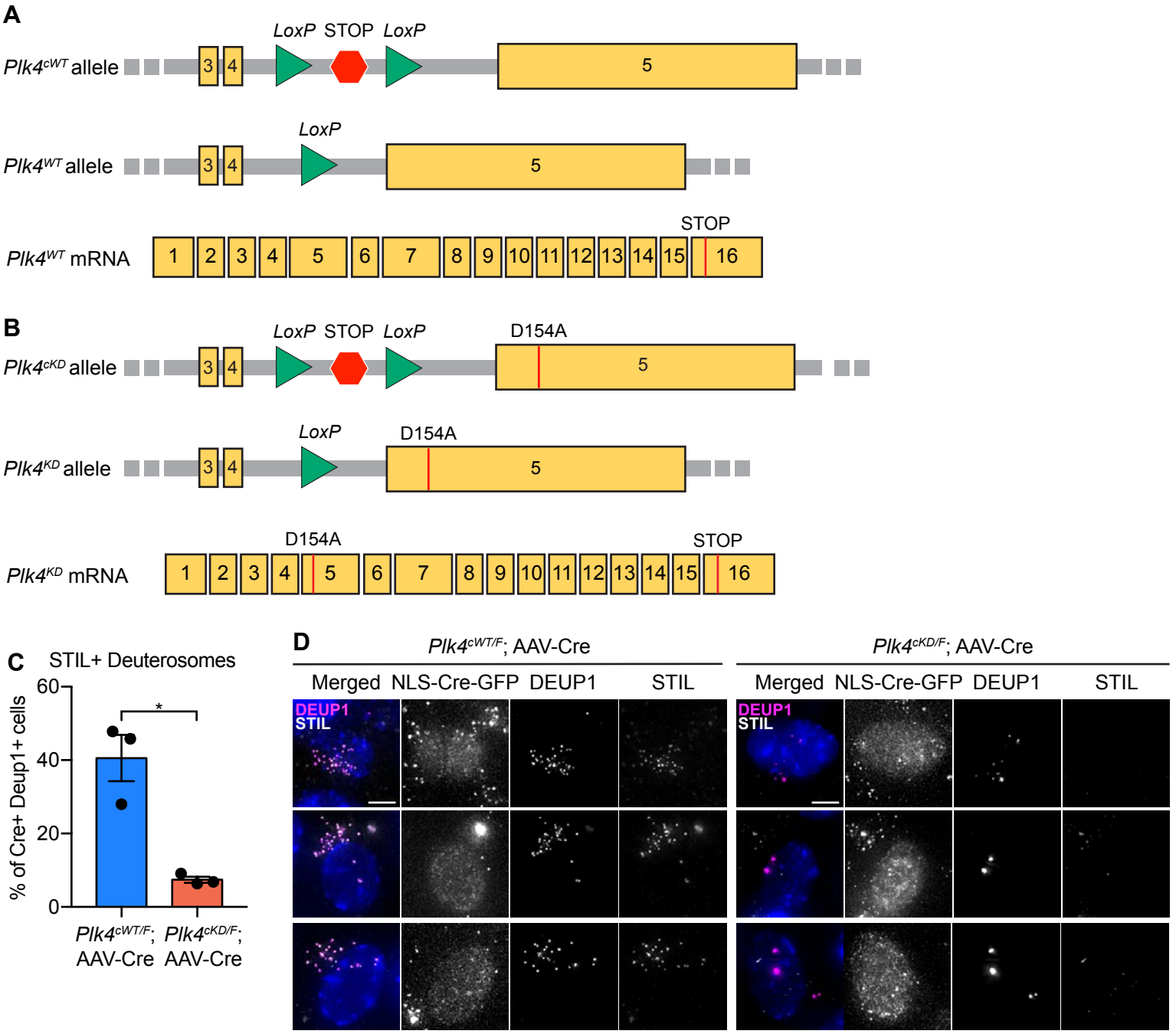
bioRxiv preprint doi: https://doi.org/10.1101/2022.06.06.494981; this version posted June 7, 2022. The copyright holder for this preprint (which was not certified by peer review) is the author/funder, who has granted bioRxiv a license to display the preprint in perpetuity. It is made available under a CC-BY 4.0 International license.

(J) Representative confocal images of mTECs treated with DMSO or 10μM centrinone at ALI 7. Cells were stained with antibodies against centrin (green), DEUP1 (magenta), and PLK4 (white).

Data information: All data represent the means ± SEM. *P < 0.05; **< 0.01; ***< 0.001; ****< 0.0001 and not significant indicates P > 0.05.

bioRxiv preprint doi: https://doi.org/10.1101/2022.06.06.494981; this version posted June 7, 2022. The copyright holder for this preprint (which was not certified by peer review) is the author/funder, who has granted bioRxiv a license to display the preprint in perpetuity. It is made available under a CC-BY 4.0 International license.

FIGURE S6



bioRxiv preprint doi: https://doi.org/10.1101/2022.06.06.494981; this version posted June 7, 2022. The copyright holder for this preprint (which was not certified by peer review) is the author/funder, who has granted bioRxiv a license to display the preprint in perpetuity. It is made available under a CC-BY 4.0 International license.

Figure S6: PLK4 kinase activity is required for STIL recruitment to deuterosomes in ependymal cells.

(A-B) Diagram of the *Plk4*^{cWT} (A) and *Plk4*^{cKD} (B) alleles showing *LoxP* sites surrounding a stop codon between exons 4 and 5 (top). The stop codon prevents transcription of either the wild-type or kinase-dead gene. Diagram of the *Plk4*^{WT} (A) and *Plk4*^{KD} (B) alleles following Cre-mediated recombination (middle). Excision of the *LoxP*-STOP-*LoxP* cassette allows for transcription. Diagram of the mRNA product created from *Plk4*^{WT} (A) and *Plk4*^{KD} (B) alleles (bottom).

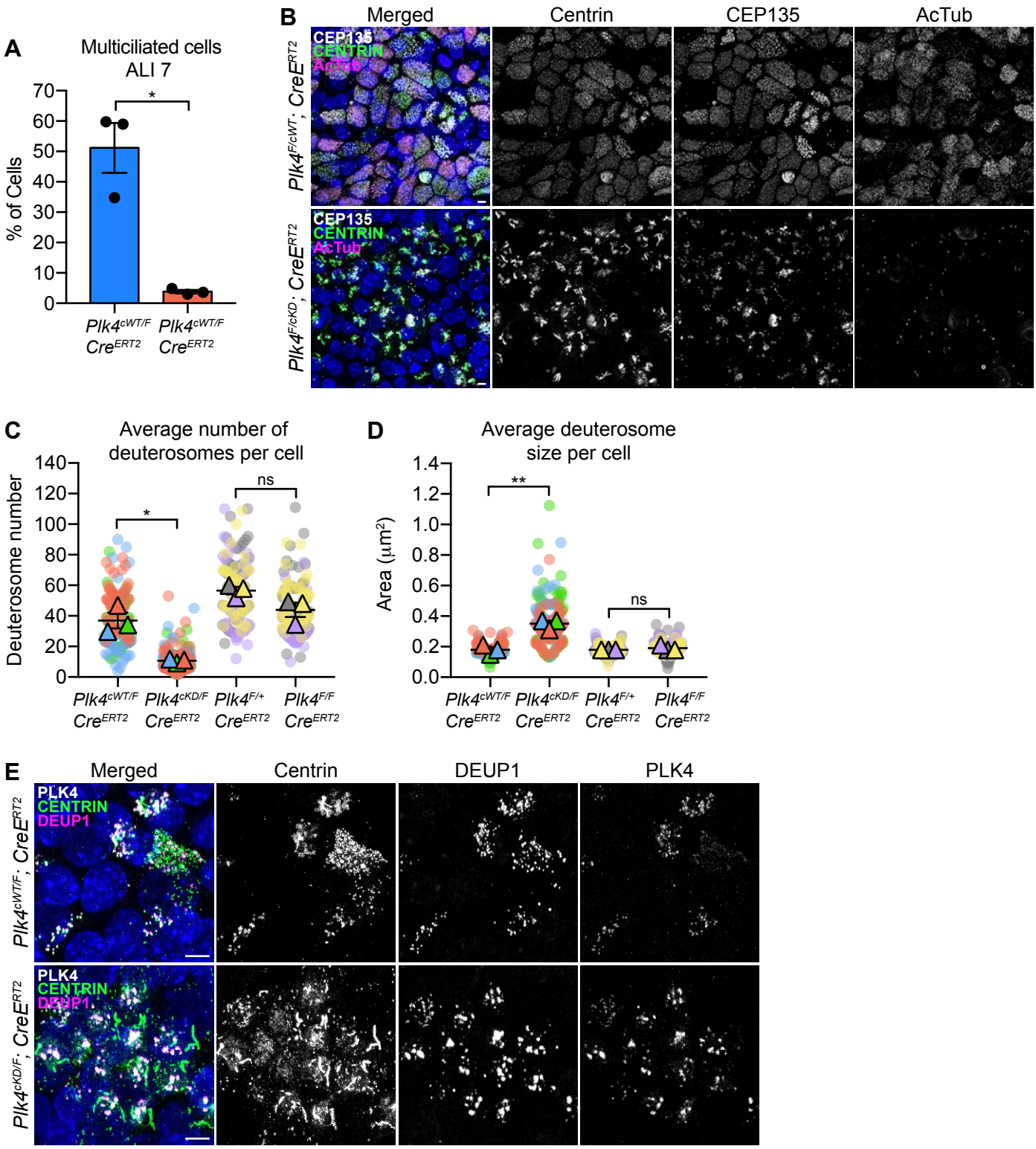
(C) Quantification of the percent of AAV-Cre transduced *Plk4*$^{cWT/F}$ and *Plk4*$^{cKD/F}$ ependymal cells with STIL+ deuterosomes. N > 3, n ≥ 50. Two-tailed Welch's t-test.

(D) Representative images of AAV-Cre transduced ependymal cells stained with antibodies against DEUP1 (magenta) and STIL (white). Scale bar = 5 μm.

Data information: All data represent the means ± SEM. *P < 0.05.

bioRxiv preprint doi: https://doi.org/10.1101/2022.06.06.494981; this version posted June 7, 2022. The copyright holder for this preprint (which was not certified by peer review) is the author/funder, who has granted bioRxiv a license to display the preprint in perpetuity. It is made available under a CC-BY 4.0 International license.

FIGURE S7



bioRxiv preprint doi: https://doi.org/10.1101/2022.06.06.494981; this version posted June 7, 2022. The copyright holder for this preprint (which was not certified by peer review) is the author/funder, who has granted bioRxiv a license to display the preprint in perpetuity. It is made available under a CC-BY 4.0 International license.

Figure S7: Centriole amplification and surface area are coupled in mTECs.

(A) Quantification of the percent of multiciliated *Plk4*$^{cWT/F}$;*Cre*^{ERT2} or *Plk4*$^{cKD/F}$;Cre^{ERT2} mTECs at ALI 7. N = 3, n > 200. Two-tailed Welch's t-test.

(B) Representative confocal images of *Plk4*$^{cWT/F}$;*Cre*^{ERT2} or *Plk4*$^{cKD/F}$;*Cre*^{ERT2} mTECs at ALI 7 stained with antibodies against CEP135 (white), Centrin (green), and acetylated-α-tubulin (magenta). Scale bar = 5 μm.

(C) Quantification of the average number of deuterosomes per cell in *Plk4*$^{cWT/F}$;Cre^{ERT2}, *Plk4*$^{cKD/F}$;*Cre*^{ERT2}, *Plk4*$^{F/+}$;*Cre*^{ERT2}, or *Plk4*$^{F/F}$;*Cre*^{ERT2} mTECs. N = 3, n ≥ 50. Two-tailed Welch's t-test.

(D) Quantification of the average deuterosome size per cell *Plk4*$^{cWT/F}$;*Cre*^{ERT2}, *Plk4*$^{cKD/F}$;*Cre*^{ERT2}, *Plk4*$^{F/+}$;*Cre*^{ERT2}, or *Plk4*$^{F/F}$;*Cre*^{ERT2} mTECs. N = 3, n ≥ 50. Two-tailed Welch's t-test.

(E) Representative confocal images of *Plk4*$^{cWT/F}$;*Cre*^{ERT2} or *Plk4*$^{cKD/F}$;*Cre*^{ERT2} mTECs at ALI 2 stained with antibodies against PLK4 (white), Centrin (green), and DEUP1 (magenta). Scale bar = 5 μm.

Data information: All data represent the means ± SEM. *P < 0.05; ***< 0.001; and not significant indicates P > 0.05.

bioRxiv preprint doi: https://doi.org/10.1101/2022.06.06.494981; this version posted June 7, 2022. The copyright holder for this preprint (which was not certified by peer review) is the author/funder, who has granted bioRxiv a license to display the preprint in perpetuity. It is made available under a CC-BY 4.0 International license.

Materials and methods

Mouse models.

Mice were housed and cared for in an AAALAC-accredited facility and the experiments were conducted in accordance with protocols approved by the Institute Animal Care and Use Committee.

Generation of Plk4$^{F/F}$ mice. Plk4$^{F/F}$ mice were generated using the *Easi*-CRISPR method (Quadros et al. 2017). A 1420 base pair single-stranded DNA donor template was injected along with pre-assembled crRNA + tracrRNA + Cas9 ribonucleoprotein (ctRNP) complexes into B6SJLF1/J mouse zygotes (JAX stock #100012). Microinjection was performed by the Johns Hopkins Transgenic Core Laboratory. The single-stranded DNA donor template and crRNA guides were synthesized by IDT. The crRNAs targeted the following DNA sequences: 5'-aagctaggactttaatactc-3' and 5'- ctgcatgtagagggaagctg-3'. The crRNA sequences were: /AltR1/rArA rGrCrU rArGrG rArCrU rUrUrA rArUrA rCrUrC rGrUrU rUrUrA rGrArG rCrUrA rUrGrC rU/AltR2/; and: /AltR1/rCrU rGrCrA rUrGrU rArGrA rGrGrG rArArG rCrUrG rGrUrU rUrUrA rGrArG rCrUrA rUrGrC rU/AltR2/. The 1420 bp donor template used was: 5'-

tacaattaggcaataaaactactgttcatatcagaaggcagtcagtatcacagctattcctcactcagccccagataacttc
gtataatgtatgctatacgaagttatcttccctctacatgcagctattagtcctttagcgatcaaacttgttcaataagtttaaaag
attatccttatactgctcagtcattatacggtctttcaaaagatccttaactattggctgtttggtgtttaatgaagttaaaacattga
cattgcttttggtgggtgaatacctgtgttgattttcatccagtgatcttctaggctttgaaagcatttctactgagtgacaacgttct
actgagtatgtttttgctcgagactgattagaggggctggctctatcagaggaatgagctctgcgcaggtatcgagaatgcg
gcctctcttctgcatcttcaatcactctcccccgtcccctactattagcttcttgttctggatttccccattgagtacaaaaattactt
ccatctcctgaagaaaagtcacttgaatttttatttttttgaaatacagtaattttatttggaagtggttgaccaaccaaaagtcttc
tgtcaagtaggctgccactcaaactggtaccagaagaggctgtaattgttgtggaaagtgtagcatgcccactatccattga
gtcctctacagtccctacgtctttactctttggtgaaggatttcgtgacatgaaaggatggtccaacacagaagacagactta
accgatctgcagggtttctacgaagtaactggtggataaggtcctgggcctctcgtgacaaaaaggctggcatttcataatc
tgccaggactactttgttcaatgtgttcttgactgtgtcagtgtcaaaaggtggtcttccaataagtaacgtataaaacatacag
cccaatgaccaaatatcagattcaagtccatgtgcacttcgagttgcaatttctggtgaaatataattaggagtcccacaga
gtgtatagtgcttttcatgtggcatattcaactgcgttgctagtccaaagtcagcaatttttatgttcatattccgcgtaagtaagat
gttagagagtgtgaggtcccggtgcaatatgccatgagaatgaagatataacattcctgtgataatctggtgcatgaagtgc

bioRxiv preprint doi: https://doi.org/10.1101/2022.06.06.494981; this version posted June 7, 2022. The copyright holder for this preprint (which was not certified by peer review) is the author/funder, who has granted bioRxiv a license to display the preprint in perpetuity. It is made available under a CC-BY 4.0 International license.

ctagctgtgaagatagaaaaagagagagcttaacaattcaaatctgggaaatttattgtttagaatacacgataaaatctag tatacacgccagagataacttcgtataatgtatgctatacgaagttattattaaagtcctagcttgcaggttagatttatcaacta aaacaccattctatcaatataatgctatctaattcccctcaagaaaactagacactcctttt-3'. Genotyping was performed with the following primers: Common Fwd: 5'-tcttgaggggaattagatagca-3', WT Rev: 5'-tgcaatatgccatgagaatga-3', LoxP Rev: 5'-ctcactcagccccagataac-3'.

Generation of Plk4^{cWT} and Plk4^{cKD} mice. Mice were created using CRISPR-Cas9 genome editing. A double-stranded DNA donor template was injected along with pre-assembled crRNA + tracrRNA + Cas9 ribonucleoprotein (ctRNP) complexes into B6SJLF1/J mouse zygotes (JAX stock #100012). Microinjection was performed by the Johns Hopkins Transgenic Core Laboratory. The donor template was amplified by PCR from plasmid DNA containing a *LoxP*-STOP-*LoxP* cassette flanked by a 1983 bp 5′ homology arm and a 1445 bp 3′ homology arm. The crRNA guide was synthesized by IDT and targeted the following DNA sequence: 5'-aagctaggactttaatactc-3'.

Centrin-GFP mice. ROSA-Neo-EGFP-Cetn1 mice. (Gt(ROSA)26Sortm1(EGFP/CETN1)Sev/J were obtained from the Jackson laboratory(Hirai et al. 2016) (strain #029363). Mice were crossed to a deleter strain to generate constitutive Centrin-GFP expression in all tissues (Centrin-GFP mice). Genotyping was performed with the following primers: Centrin-GFP 1: 5'-AAAGTCGCTCTGAGTTGTTAT-3', Centrin-GFP 2: 5'-GCGAAGAGTTTGTCCTCAACC-3', Centrin-GFP 3: 5'-GGAGCGGGAGAAATGGATATG-3'.

Rosa-Cre^{ERT2} mice. *R26-CreERT2* mice (B6.129-Gt(ROSA)26Sortm1(cre/ERT2)Tyj/J) were obtained from the Jackson laboratory (Ventura et al. 2007) (strain #008463). Genotyping was performed with the following primers: Reaction 1: WT Fwd: 5'-CTGGCTTCTGAGGACCG-3', WT Rev: 5'-CCGAAAATCTGTGGGAAGTC-3', Reaction 2: Mut Fwd: 5'-CGTGATCTGCAACTCCAGTC-3', Mut Rev: 5'-AGGCAAATTTTGGTGTACGG-3'.

bioRxiv preprint doi: https://doi.org/10.1101/2022.06.06.494981; this version posted June 7, 2022. The copyright holder for this preprint (which was not certified by peer review) is the author/funder, who has granted bioRxiv a license to display the preprint in perpetuity. It is made available under a CC-BY 4.0 International license.

Nestin-Cre mice. Nestin-Cre mice were obtained from The Jackson Laboratory (stock #003771) (Tronche et al. 1999). The following primers were used for genotyping: Nestin-Cre Fwd 5'-ATTGCTGTCACTTGGTCGTGGC-3'; Nestin-Cre Rev 5'-GGAAAATGCTTCTGTCCGTTTGC-3'.

Usp28$^{F/F}$ mice. *Usp28$^{F/-}$* mice were obtained from the laboratory M. Eilers (University of Wuerzburg, Germany) (Diefenbacher et al. 2014). The following primers were used for genotyping: Usp28 Common Fwd 1718 27 5'-GAGGCTTGAGTTATGACTGG-3'; Usp28 WT Rev 1718 m28 5'-AGAACACCTGCTGCTTAAGC-3'; Usp28 Del Rev 5'-TCCCCCAAGAGTGTTTTCAC-3'.

Cell culture.

Primary cells. mTEC cultures were harvested and grown as previously described (You and Brody 2013). Briefly, tracheas were harvested from mice that were between 3 weeks and 12 months old. Tracheas were then incubated overnight in Pronase (Roche) at 4 °C. Tracheal cells were dissociated by enzymatic and mechanical digestion the following day. The cells were plated onto 0.4-μm Falcon transwell membranes (Transwell, Corning). Once the cells were confluent (proliferation day 3), 2.5 μM 4-Hydroxytamoxifen (4OHT) was added to the apical and basal chambers. On proliferation day 5, the medium from the apical chamber was removed and the basal medium was replaced with NuSerum medium containing 2.5 μM 4OHT. This time point is considered air-liquid interface day 0 (ALI 0). The basal media was changed every 2 days and the 4OHT was replenished. Cells were allowed to differentiate until needed for analysis (ALI day 3, 7, or 21). For cultures analyzed at ALI 21. 4OHT was supplied to the media until ALI 7.

For the mouse ependymal cell cultures, brains were dissected from P0–P2 mice, dissociated and cultured as previously described (Delgehyr et al. 2015). Briefly, the mice were sacrificed by decapitation. The brains were dissected in Hank's solution (10% HBSS, 5% HEPES, 5% sodium bicarbonate and 1% penicillin/streptomycin (P/S) in pure water) and the telencephalon was manually cut into pieces, followed by

bioRxiv preprint doi: https://doi.org/10.1101/2022.06.06.494981; this version posted June 7, 2022. The copyright holder for this preprint (which was not certified by peer review) is the author/funder, who has granted bioRxiv a license to display the preprint in perpetuity. It is made available under a CC-BY 4.0 International license.

enzymatic digestion (DMEM GlutaMAX 1% P/S, 3% papain (Worthington 3126), 1.5% 10 mg ml^{-1} DNAse and 2.4% 12 mg ml^{-1} cystein) for 45min at 37 °C in a water bath. The digestion was stopped by the addition of a solution of trypsin inhibitors (Leibovitz's L15 medium, 10% 1 mg ml^{-1} trypsin inhibitor (Worthington) and 2% 10 mg ml^{-1} DNAse). The cells were then washed in L15 medium and resuspended in DMEM GlutaMAX supplemented with 10% fetal bovine serum (FBS) and 1% P/S in a poly-l-lysine-coated flask. The ependymal progenitors were allowed to proliferate for 4–5d, until confluence was reached, before being incubated overnight with shaking (250 r.p.m.), and then re-plated at a density of 7×10^4 cells cm^{-2} (differentiation day -1) in DMEM GlutaMAX, 10% FBS and 1% P/S on poly-l-lysine-coated coverslips. The following day, the medium was replaced with serum-free DMEM GlutaMAX 1% P/S to trigger ependymal differentiation in vitro (differentiation day 0).

Adeno-associated virus transduction of ependymal cells. At differentiation day 0 ependymal cells were washed 2x with PBS. pAAV.CMV.HI.eGFP-Cre.WPRE.SV40 (Addgene, cat. No. 105545-AAV1) was resuspended in DMEM GlutaMAX 1% P/S at an MOI of 100,000. 250μL of viral solution was added per well. Cells were incubated with virus for 4-5 hours, and then the viral media was replaced with 1mL of DMEM GlutaMAX with 1% P/S.

Processing of cells and tissues for immunofluorescence microscopy.
mTEC cultures. Membranes were fixed in 100% ice-cold methanol for 10 minutes at −20°C. The membranes were washed 3× with PBS for 5 min each. The membranes were then blocked at room temperature for 1h in PBS with 0.2M Glycine, 2.5% FBS, and 0.1% Triton X-100. The membranes were cut in half and incubated with primary antibodies diluted in blocking buffer for 1h at room temperature. Next, the membranes were washed 3× in PBS for 5 min each and incubated for 45 min at room temperature with secondary antibodies and DAPI diluted in blocking buffer. The membranes were again washed 3× in PBS for 5 min each and mounted onto slides using ProLong Gold Antifade (Invitrogen). Images of stained mTECs were obtained using an SP8 (Leica

bioRxiv preprint doi: https://doi.org/10.1101/2022.06.06.494981; this version posted June 7, 2022. The copyright holder for this preprint (which was not certified by peer review) is the author/funder, who has granted bioRxiv a license to display the preprint in perpetuity. It is made available under a CC-BY 4.0 International license.

Microsystems) confocal microscope. Images were collected using a Leica 63× 1.40 NA oil objective at 0.5 μM z-sections.

Ependymal cell cultures. Cells were grown on 12-mm glass coverslips as described above and fixed for 10min in either 4% PFA (for FOXJ1) at room temperature or 100% ice-cold methanol at −20°C. The samples were blocked in PBS with 0.2% Triton X-100 and 10% FBS before incubation with the primary and secondary antibodies. The cells were counterstained with DAPI (10μg ml^{-1}; Sigma) and mounted in ProLong Gold Antifade (Invitrogen). Immunofluorescence images were collected using a Deltavision Elite system (GE Healthcare) controlling a Scientific CMOS camera (pco.edge 5.5). Acquisition parameters were controlled by SoftWoRx suite (GE Healthcare). Images were collected at room temperature using an Olympus 60× 1.42 NA oil objective at 0.2 mM z-sections and subsequently deconvolved in SoftWoRx suite.

Brains for the ex vivo imaging of ependymal cells. To isolate the lateral wall for immunofluorescence, brains from P21 *Plk4$^{F/F}$;Usp28$^{F/F}$;*Nestin-Cre mice and littermate controls were dissected as described previously (Mirzadeh et al. 2010). Animals were sacrificed by cervical dislocation and the head was removed. The brain was dissected out of the skull and placed in a petri dish with PBS. The remainder of the dissection was performed under the stereomicroscope. First, the olfactory bulbs were dissected away from the brain. The brain was then divided along the intrahemispheric fissure and a coronally-oriented cut was made at the posterior-most aspect of the interhemispheric fissure, allowing the caudal hippocampus to be visualized in cross-section. The hippocampus was then released from the overlying cortex. The lateral wall then completely exposed by removing any overhanging cortex dorsally and the thalamus ventrally. The dissected brains were then fixed overnight in 4% PFA in PBST (PBS + 0.1% Triton X-100) at 4°C. The following day, brains were washed 3x in PBST for 20 minutes at room temperature, and then incubated with 30% sucrose in PBS for 24 hours at 4°C. Brains were embedded in O.C.T. medium and frozen for cryosectioning. 20 μm brain sections were cut using a Leica CM3050 cryostat and collected on Superfrost microscope slides (Thermo Fisher Scientific). For immunohistochemistry staining, the

bioRxiv preprint doi: https://doi.org/10.1101/2022.06.06.494981; this version posted June 7, 2022. The copyright holder for this preprint (which was not certified by peer review) is the author/funder, who has granted bioRxiv a license to display the preprint in perpetuity. It is made available under a CC-BY 4.0 International license.

brain sections were rehydrated with PBS for 5 minutes at room temperature, blocked and permeabilized with blocking solution (10% donkey serum (Sigma Aldrich), 0.5% Triton X-100 in PBS) for 1 hour at room temperature, and incubated with the respective primary antibodies diluted in blocking solution for 12 h at 4°C. Following primary antibody staining, the tissue slides were washed 3 times with PBS + 0.5% Triton X-100 and incubated with secondary antibodies and DAPI diluted in blocking solution for 1 h at room temperature. Following secondary antibody staining, the tissue slides were washed three times with PBS + 0.5% Triton X-100 before mounting. Secondary antibodies were conjugated to Alexa Fluor 488, 555, or 647 (Thermo Fisher Scientific, 1:500). Images of stained sections were obtained using an SP8 (Leica Microsystems) confocal microscope. Images were collected using a Leica 63× 1.40 NA oil objective at 0.5 μM z-sections.

Brains for analysis of telencephalon area and ex vivo imaging of NPCs. For analysis of embryonic brain sections, timed pregnant females carrying the respective transgenes were anesthetized with isoflurane before cervical dislocation. The heads of the embryos were removed and rinsed with ice-cold PBS, followed by incubation in 4% paraformaldehyde in PBS overnight at 4°C. The next day, the brains were dissected out of the skulls and rinsed three times with PBS before being imaged using a MU1003 digital camera attached to a dissecting microscope (Amscope). The brains were then incubated in 30% sucrose at 4°C for 24 h. Brains were embedded in O.C.T medium and frozen for cryosectioning. 20 μm brain sections were cut using a Leica CM3050 cryostat and collected on Superfrost microscope slides (Thermo Fisher Scientific). Tissue staining was performed, and images were collected as described above.

Ultrastructure expansion microscopy (U-ExM).

Ependymal cells. U-ExM was carried out as previously described (Gambarotto et al. 2021). Coverslips with unfixed cells were incubated in a solution of 0.7% formaldehyde with 1% acrylamide in PBS for 5 h at 37 °C. Gelation was carried out via incubation of coverslips with cells facing down with 35 μl of U-ExM MS composed of 19% (wt/wt) sodium acrylate, 10% (wt/wt) acrylamide, 0.1% (wt/wt) N,N′-methylenbisacrylamide

bioRxiv preprint doi: https://doi.org/10.1101/2022.06.06.494981; this version posted June 7, 2022. The copyright holder for this preprint (which was not certified by peer review) is the author/funder, who has granted bioRxiv a license to display the preprint in perpetuity. It is made available under a CC-BY 4.0 International license.

(BIS) in PBS supplemented with 0.5% APS and 0.5% TEMED, on Parafilm in a pre-cooled humid chamber. Gelation proceeded for 10 min on ice, and then samples were incubated at 37 °C in the dark for 1 h. A 4mm biopsy puncher (Integra; 33-34-P/25) was used to create one punch per coverslip. Punches were transferred into 1.5-ml Eppendorf tubes containing 1mL denaturation buffer (200 mM SDS, 200 mM NaCl, and 50 mM Tris in ultrapure water, pH 9) and incubated at 95 °C for 1 hour. After denaturation, gels were placed in beakers filled with ddH2O for the first expansion. Water was exchanged at least twice every 30 min at RT, and then gels were incubated overnight in ddH2O. Next, to remove excess water before incubation with primary antibody solution, gels were placed in PBS two times for 15 min. Incubation with primary antibody diluted in 2% PBS/BSA was carried out at 37 °C for 2.5h, with gentle shaking. Gels were then washed in PBST three times for 10 min with shaking and subsequently incubated with secondary antibody solution diluted in 2% PBS/BSA for 2.5 h at 37 °C with gentle shaking. Gels were then washed in PBST three times for 10 min with shaking and finally placed in beakers filled with ddH2O for expansion. Water was exchanged at least twice every 30 min, and then gels were incubated in ddH2O overnight. Gel expanded between 4.0× and 4.5× according to SA purity.

mTEC cultures. U-ExM was carried out as previously described with a few modifications (Gambarotto et al. 2021; Kong and Loncarek 2021). Transwell filters containing mTECs were fixed in freshly made 4% PFA in PBS for 1 hour at RT. Filters were then incubated in a solution of 30% acrylamide with 4% formaldehyde at 37 °C for 16 hours. Filters were washed 3x with PBS for 10 minutes at RT. Filters were cut out of their transwell holders and placed cell-side up on a parafilm-coated petri dish on ice. After cooling for 20 minutes, complete polymerization mixture was added to the filters (20% acrylamide, 0.04% bisacrylamide, 7% sodium acrylate, 0.5% TEMED, 0.5% ammonium persulfate, in 1× PBS) and a coverslip was placed on top. Samples were kept on ice for 20 minutes, and then incubated at RT for 1 hour. One punch was cut from each filter using a 4-mm biopsy puncher. Punches were boiled in SDS buffer (0.2M NaCl, 0.05M Tris-HCl, 5% SDS) for one hour. Punches were washed 10x 20 minutes in PBS at RT. Immunolabeling and expansion of samples was performed as described above.

bioRxiv preprint doi: https://doi.org/10.1101/2022.06.06.494981; this version posted June 7, 2022. The copyright holder for this preprint (which was not certified by peer review) is the author/funder, who has granted bioRxiv a license to display the preprint in perpetuity. It is made available under a CC-BY 4.0 International license.

Antibodies.

The staining of cells and tissues was performed with the following primary antibodies: rabbit polyclonal anti-CEP164 (1:1,000; EMD Millipore, ABE2621), mouse monoclonal acetylated-α-tubulin (1:1,000 IF, 1:500 IHC; Cell Signaling Technologies, cat. no. 12152), rat polyclonal anti-ZO-1 (1:1,000; Thermo Fisher Scientific, 14-9776-82), rabbit polyclonal anti-DEUP1 no. 1 (1:1,000; homemade, raised against the full-length protein(Mercey et al. 2019)), mouse anti-SAS6 (1:1000; Santa Cruz, sc-81431), rabbit anti-PCNT (1:1,000, Abcam ab4448), mouse monoclonal anti-FOXJ1 (1:1,000 Thermo Fisher 14-9965-82), rabbit anti-PLK4 (homemade(Moyer et al. 2015) against hPLK4 a.a. 510–970, 1:1,000) rabbit anti-STIL (homemade(Moyer et al. 2015) raised against the peptide VGTFLDVKRLRQLPKLF 1:1,000), rabbit anti-CEP135, (homemade, raised against a.a. 649-1140, rabbit anti- acetylated-α-Tubulin (1:1,000 IF, 1:500 IHC; Cell Signaling Technologies, cat. No. 5335), rabbit anti-CNTROB (1:1,000; Atlas Antibodies HPA023321), rabbit anti-CEP152 (homemade, raised against a.a. 491-810), rabbit anti-CDK5RAP2 (1:1,000; Bethyl, BETIHC-00063), Goat polyclonal anti-CEP192 (homemade(Moyer and Holland 2019) raised against a.a. 1-211), Goat anti-γ-Tubulin (homemade(Levine et al. 2017), polyclonal, raised against the peptide CDEYHAATRPDYISWGTQEQ, 1:1,000). The secondary antibodies were conjugated to Alexa Fluor 488, 555 or 650 (Life Technologies).

Quantification of centriole number in fixed samples.

Ependymal cells. Regions that contained a high density of MCCs were selected. At least three fields of view were selected per sample. In *Plk4*$^{F/F}$; AAV-Cre ependymal cell samples all DEUP1+ cells within those fields of view were counted. In control ependymal cell samples, all MCCs in the disengagement phase of centriole amplification were counted. Cells for which individual centrioles could not be resolved were excluded from our analysis. The CEP135 foci in each cell were quantified using a semi-automated ImageJ macro. A circle was drawn around all CEP135 foci in each cell.

bioRxiv preprint doi: https://doi.org/10.1101/2022.06.06.494981; this version posted June 7, 2022. The copyright holder for this preprint (which was not certified by peer review) is the author/funder, who has granted bioRxiv a license to display the preprint in perpetuity. It is made available under a CC-BY 4.0 International license.

A threshold was applied to each image, and CEP135 intensity maxima were identified and counted by ImageJ.

mTEC cultures. Measurements of apical area were made using ImageJ. A perimeter was drawn around the apical area of individual cells by hand using the polygon selection tool and ZO1 as a marker, and the measurement function of ImageJ was used to measure the apical area. Centriole number per cell was quantified as described above.

Quantifications of fluorescence intensities.

Regions that contained a high density of MCCs were selected. At least three fields of view were selected per sample and all DEUP1+ cells were analyzed. PLK4 intensity on deuterosome measurements were made using a semi-automated ImageJ macro. A circle was drawn to encompass all deuterosomes for a given cell. Deuterosomes were identified by DEUP1 signal based on a pre-set threshold which was kept the same throughout all images in a replicate. Signal intensity of PLK4 (raw integrated density) was then measured within the DEUP1 threshold. For a given cell, the background-subtracted intensity within each thresholded region was added together to calculate the total PLK4 intensity on deuterosomes per cell. The SAS6 and STIL intensity measurements were collected in the same way.

Quantifications of deuterosome number and area.

Quantification of deuterosome number and area was performed using a semi-automated ImageJ macro. Cells were manually segmented and deuterosomes were identified by automated thresholding of the DEUP1 signal. DEUP1 intensity maxima were used to count deuterosome numbers. The area of the thresholded region was divided by the deuterosome number to calculate the average deuterosome area.

Fluorescence recovery after photobleaching.

To prepare cells for photobleaching experiments, WT and PLK4 KO mTECs expressing GFP-Centrin were isolated and differentiated as described above. On ALI day 3, the

bioRxiv preprint doi: https://doi.org/10.1101/2022.06.06.494981; this version posted June 7, 2022. The copyright holder for this preprint (which was not certified by peer review) is the author/funder, who has granted bioRxiv a license to display the preprint in perpetuity. It is made available under a CC-BY 4.0 International license.

filters with adhered cells were cut out from the transwell insert and inverted onto a glass coverslip with a drop of differentiation media. A plastic ring was placed on top of the filter to keep it in contact with the coverslip. Cells were imaged on a Leica Sp8 inverted microscope using a 63x/1.4 NA objective. An ROI was drawn around all or part of a GFP-Centrin signal at the centrioles or aggregates and photobleached to approximately 80% of the pre-bleach fluorescence intensity with 10 pulses of 488 nm laser light (1039 ms exposure). A Z-series of 13 planes (0.5 µm step size) was acquired immediately before and after bleaching. GFP-Centrin fluorescence intensities within the bleached ROI were measured using ImageJ. The first post-bleach intensity was subtracted from the pre-bleach and post-bleach values and then normalized to give the percentage of the pre-bleach intensity

bioRxiv preprint doi: https://doi.org/10.1101/2022.06.06.494981; this version posted June 7, 2022. The copyright holder for this preprint (which was not certified by peer review) is the author/funder, who has granted bioRxiv a license to display the preprint in perpetuity. It is made available under a CC-BY 4.0 International license.

Acknowledgments

This work was supported by the National Institutes of Health grants R01GM114119 and R01GM133897 (to A.J.H).

Author contributions

A.J.H. and G.M.L. conceived the project. G.M.L. performed and analyzed the majority of the experiments and prepared the figures. C.G.D. assisted with mouse husbandry and some analysis. M.A.S. assisted with mouse husbandry. A.L.M measured telencephalon area and quantified centriole number in NPCs. C.J performed the FRAP analysis. A.J.H. and G.L. wrote the manuscript. All authors edited the manuscript.

bioRxiv preprint doi: https://doi.org/10.1101/2022.06.06.494981; this version posted June 7, 2022. The copyright holder for this preprint (which was not certified by peer review) is the author/funder, who has granted bioRxiv a license to display the preprint in perpetuity. It is made available under a CC-BY 4.0 International license.

References

Al Jord A, Lemaitre AI, Delgehyr N, Faucourt M, Spassky N, Meunier A. 2014. Centriole amplification by mother and daughter centrioles differs in multiciliated cells. *Nature* **516**: 104-107.

Al Jord A, Shihavuddin A, Servignat d'Aout R, Faucourt M, Genovesio A, Karaiskou A, Sobczak-Thepot J, Spassky N, Meunier A. 2017. Calibrated mitotic oscillator drives motile ciliogenesis. *Science*.

Anderson RG, Brenner RM. 1971. The formation of basal bodies (centrioles) in the Rhesus monkey oviduct. *J Cell Biol* **50**: 10-34.

Bettencourt-Dias M, Rodrigues-Martins A, Carpenter L, Riparbelli M, Lehmann L, Gatt MK, Carmo N, Balloux F, Callaini G, Glover DM. 2005. SAK/PLK4 is required for centriole duplication and flagella development. *Curr Biol* **15**: 2199-2207.

Brenner RM. 1969. Renewal of oviduct cilia during the menstrual cycle of the rhesus monkey. *Fertil Steril* **20**: 599-611.

Cizmecioglu O, Arnold M, Bahtz R, Settele F, Ehret L, Haselmann-Weiss U, Antony C, Hoffmann I. 2010. Cep152 acts as a scaffold for recruitment of Plk4 and CPAP to the centrosome. *J Cell Biol* **191**: 731-739.

Delgehyr N, Meunier A, Faucourt M, Bosch Grau M, Strehl L, Janke C, Spassky N. 2015. Ependymal cell differentiation, from monociliated to multiciliated cells. *Methods Cell Biol* **127**: 19-35.

Diefenbacher ME, Popov N, Blake SM, Schulein-Volk C, Nye E, Spencer-Dene B, Jaenicke LA, Eilers M, Behrens A. 2014. The deubiquitinase USP28 controls intestinal homeostasis and promotes colorectal cancer. *J Clin Invest* **124**: 3407-3418.

Dzhindzhev NS, Tzolovsky G, Lipinszki Z, Schneider S, Lattao R, Fu J, Debski J, Dadlez M, Glover DM. 2014. Plk4 phosphorylates Ana2 to trigger Sas6 recruitment and procentriole formation. *Curr Biol* **24**: 2526-2532.

Florea BI, van der Sandt IC, Schrier SM, Kooiman K, Deryckere K, de Boer AG, Junginger HE, Borchard G. 2001. Evidence of P-glycoprotein mediated apical to basolateral transport of flunisolide in human broncho-tracheal epithelial cells (Calu-3). *Br J Pharmacol* **134**: 1555-1563.

Gambarotto D, Hamel V, Guichard P. 2021. Ultrastructure expansion microscopy (U-ExM). *Methods Cell Biol* **161**: 57-81.

Habedanck R, Stierhof YD, Wilkinson CJ, Nigg EA. 2005. The Polo kinase Plk4 functions in centriole duplication. *Nat Cell Biol* **7**: 1140-1146.

bioRxiv preprint doi: https://doi.org/10.1101/2022.06.06.494981; this version posted June 7, 2022. The copyright holder for this preprint (which was not certified by peer review) is the author/funder, who has granted bioRxiv a license to display the preprint in perpetuity. It is made available under a CC-BY 4.0 International license.

Hatch EM, Kulukian A, Holland AJ, Cleveland DW, Stearns T. 2010. Cep152 interacts with Plk4 and is required for centriole duplication. *J Cell Biol* **191**: 721-729.

Hirai M, Chen J, Evans SM. 2016. Generation and Characterization of a Tissue-Specific Centrosome Indicator Mouse Line. *Genesis* **54**: 286-296.

Hoh RA, Stowe TR, Turk E, Stearns T. 2012. Transcriptional program of ciliated epithelial cells reveals new cilium and centrosome components and links to human disease. *PLoS One* **7**: e52166.

Holland AJ, Lan W, Niessen S, Hoover H, Cleveland DW. 2010. Polo-like kinase 4 kinase activity limits centrosome overduplication by autoregulating its own stability. *J Cell Biol* **188**: 191-198.

Kalnins VI, Porter KR. 1969. Centriole replication during ciliogenesis in the chick tracheal epithelium. *Zeitschrift fur Zellforschung und mikroskopische Anatomie* **100**: 1-30.

Kim TS, Park JE, Shukla A, Choi S, Murugan RN, Lee JH, Ahn M, Rhee K, Bang JK, Kim BY et al. 2013. Hierarchical recruitment of Plk4 and regulation of centriole biogenesis by two centrosomal scaffolds, Cep192 and Cep152. *Proc Natl Acad Sci U S A* **110**: E4849-4857.

Klos Dehring DA, Vladar EK, Werner ME, Mitchell JW, Hwang P, Mitchell BJ. 2013. Deuterosome-mediated centriole biogenesis. *Dev Cell* **27**: 103-112.

Kong D, Loncarek J. 2021. Analyzing Centrioles and Cilia by Expansion Microscopy. *Methods Mol Biol* **2329**: 249-263.

Kratz AS, Barenz F, Richter KT, Hoffmann I. 2015. Plk4-dependent phosphorylation of STIL is required for centriole duplication. *Biol Open* **4**: 370-377.

Kulkarni S, Marquez J, Date P, Ventrella R, Mitchell BJ, Khokha MK. 2021. Mechanical stretch scales centriole number to apical area via Piezo1 in multiciliated cells. *Elife* **10**.

Lambrus BG, Daggubati V, Uetake Y, Scott PM, Clutario KM, Sluder G, Holland AJ. 2016. A USP28-53BP1-p53-p21 signaling axis arrests growth after centrosome loss or prolonged mitosis. *The Journal of cell biology* **214**: 143-153.

Levine MS, Bakker B, Boeckx B, Moyett J, Lu J, Vitre B, Spierings DC, Lansdorp PM, Cleveland DW, Lambrechts D et al. 2017. Centrosome Amplification Is Sufficient to Promote Spontaneous Tumorigenesis in Mammals. *Developmental Cell* **40**: 313-322.e315.

Mercey O, Levine MS, LoMastro GM, Rostaing P, Brotslaw E, Gomez V, Kumar A, Spassky N, Mitchell BJ, Meunier A et al. 2019. Massive centriole production can

bioRxiv preprint doi: https://doi.org/10.1101/2022.06.06.494981; this version posted June 7, 2022. The copyright holder for this preprint (which was not certified by peer review) is the author/funder, who has granted bioRxiv a license to display the preprint in perpetuity. It is made available under a CC-BY 4.0 International license.

occur in the absence of deuterosomes in multiciliated cells. *Nat Cell Biol* **21**: 1544-1552.

Mirzadeh Z, Doetsch F, Sawamoto K, Wichterle H, Alvarez-Buylla A. 2010. The subventricular zone en-face: wholemount staining and ependymal flow. *J Vis Exp*.

Montenegro Gouveia S, Zitouni S, Kong D, Duarte P, Ferreira Gomes B, Sousa AL, Tranfield EM, Hyman A, Loncarek J, Bettencourt-Dias M. 2018. PLK4 is a microtubule-associated protein that self-assembles promoting de novo MTOC formation. *J Cell Sci* **132**.

Moyer TC, Clutario KM, Lambrus BG, Daggubati V, Holland AJ. 2015. Binding of STIL to Plk4 activates kinase activity to promote centriole assembly. *J Cell Biol* **209**: 863-878.

Moyer TC, Holland AJ. 2019. PLK4 promotes centriole duplication by phosphorylating STIL to link the procentriole cartwheel to the microtubule wall. *Elife* **8**.

Nanjundappa R, Kong D, Shim K, Stearns T, Brody SL, Loncarek J, Mahjoub MR. 2019. Regulation of cilia abundance in multiciliated cells. *Elife* **8**.

Nigg EA, Holland AJ. 2018. Once and only once: mechanisms of centriole duplication and their deregulation in disease. *Nat Rev Mol Cell Biol* **19**: 297-312.

Ohta M, Ashikawa T, Nozaki Y, Kozuka-Hata H, Goto H, Inagaki M, Oyama M, Kitagawa D. 2014. Direct interaction of Plk4 with STIL ensures formation of a single procentriole per parental centriole. *Nat Commun* **5**: 5267.

Park JE, Zhang L, Bang JK, Andresson T, DiMaio F, Lee KS. 2019. Phase separation of Polo-like kinase 4 by autoactivation and clustering drives centriole biogenesis. *Nat Commun* **10**: 4959.

Park SY, Park JE, Kim TS, Kim JH, Kwak MJ, Ku B, Tian L, Murugan RN, Ahn M, Komiya S et al. 2014. Molecular basis for unidirectional scaffold switching of human Plk4 in centriole biogenesis. *Nat Struct Mol Biol* **21**: 696-703.

Phan TP, Maryniak AL, Boatwright CA, Lee J, Atkins A, Tijhuis A, Spierings DC, Bazzi H, Foijer F, Jordan PW et al. 2021. Centrosome defects cause microcephaly by activating the 53BP1-USP28-TP53 mitotic surveillance pathway. *Embo J* **40**: e106118.

Quadros RM, Miura H, Harms DW, Akatsuka H, Sato T, Aida T, Redder R, Richardson GP, Inagaki Y, Sakai D et al. 2017. Easi-CRISPR: a robust method for one-step generation of mice carrying conditional and insertion alleles using long ssDNA donors and CRISPR ribonucleoproteins. *Genome Biol* **18**: 92.

bioRxiv preprint doi: https://doi.org/10.1101/2022.06.06.494981; this version posted June 7, 2022. The copyright holder for this preprint (which was not certified by peer review) is the author/funder, who has granted bioRxiv a license to display the preprint in perpetuity. It is made available under a CC-BY 4.0 International license.

Reiter JF, Leroux MR. 2017. Genes and molecular pathways underpinning ciliopathies. *Nat Rev Mol Cell Biol* **18**: 533-547.

Revinski DR, Zaragosi LE, Boutin C, Ruiz-Garcia S, Deprez M, Thome V, Rosnet O, Gay AS, Mercey O, Paquet A et al. 2018. CDC20B is required for deuterosome-mediated centriole production in multiciliated cells. *Nat Commun* **9**: 4668.

Sonnen KF, Gabryjonczyk AM, Anselm E, Stierhof YD, Nigg EA. 2013. Human Cep192 and Cep152 cooperate in Plk4 recruitment and centriole duplication. *J Cell Sci* **126**: 3223-3233.

Sorokin SP. 1968. Reconstructions of centriole formation and ciliogenesis in mammalian lungs. *J Cell Sci* **3**: 207-230.

Spassky N, Meunier A. 2017. The development and functions of multiciliated epithelia. *Nat Rev Mol Cell Biol* **18**: 423-436.

Steinman RM. 1968. An electron microscopic study of ciliogenesis in developing epidermis and trachea in the embryo of Xenopus laevis. *Am J Anat* **122**: 19-55.

Terre B, Lewis M, Gil-Gomez G, Han Z, Lu H, Aguilera M, Prats N, Roy S, Zhao H, Stracker TH. 2019. Defects in efferent duct multiciliogenesis underlie male infertility in GEMC1-, MCIDAS- or CCNO-deficient mice. *Development* **146**.

Tronche F, Kellendonk C, Kretz O, Gass P, Anlag K, Orban PC, Bock R, Klein R, Schutz G. 1999. Disruption of the glucocorticoid receptor gene in the nervous system results in reduced anxiety. *Nat Genet* **23**: 99-103.

Ventura A, Kirsch DG, McLaughlin ME, Tuveson DA, Grimm J, Lintault L, Newman J, Reczek EE, Weissleder R, Jacks T. 2007. Restoration of p53 function leads to tumour regression in vivo. *Nature* **445**: 661-665.

Yamamoto S, Kitagawa D. 2018. Self-organization of Plk4 regulates symmetry breaking in centriole duplication. *bioRxiv*.

You Y, Brody SL. 2013. Culture and differentiation of mouse tracheal epithelial cells. *Methods Mol Biol* **945**: 123-143.

Yuan S, Liu Y, Peng H, Tang C, Hennig GW, Wang Z, Wang L, Yu T, Klukovich R, Zhang Y et al. 2019. Motile cilia of the male reproductive system require miR-34/miR-449 for development and function to generate luminal turbulence. *Proc Natl Acad Sci U S A* **116**: 3584-3593.

Zaragosi LE, Deprez M, Barbry P. 2020. Using single-cell RNA sequencing to unravel cell lineage relationships in the respiratory tract. *Biochem Soc Trans* **48**: 327-336.

bioRxiv preprint doi: https://doi.org/10.1101/2022.06.06.494981; this version posted June 7, 2022. The copyright holder for this preprint (which was not certified by peer review) is the author/funder, who has granted bioRxiv a license to display the preprint in perpetuity. It is made available under a CC-BY 4.0 International license.

Zhao H, Chen Q, Fang C, Huang Q, Zhou J, Yan X, Zhu X. 2019. Parental centrioles are dispensable for deuterosome formation and function during basal body amplification. *EMBO Rep* **20**.

Zhao H, Chen Q, Li F, Cui L, Xie L, Huang Q, Liang X, Zhou J, Yan X, Zhu X. 2021. Fibrogranular materials function as organizers to ensure the fidelity of multiciliary assembly. *Nat Commun* **12**: 1273.

Zhao H, Zhu L, Zhu Y, Cao J, Li S, Huang Q, Xu T, Huang X, Yan X, Zhu X. 2013. The Cep63 paralogue Deup1 enables massive de novo centriole biogenesis for vertebrate multiciliogenesis. *Nat Cell Biol* **15**: 1434-1444.